ISSN 0737-5352
CIRA
Paper No. 4

A Modeling Study of Visibility in the Grand Canyon

Michael Jeffrey Weissbluth
and Stephen K. Cox

CIRA

Cooperative Institute for Research in the Atmosphere

Colorado State University
Foothills Campus
Fort Collins, Colorado 80523

Colorado State University / National Oceanic and Atmospheric Administration

A MODELING STUDY OF VISIBILITY IN THE GRAND CANYON

by

Michael Jeffrey Weissbluth

and

Stephen K. Cox

Research Support by

National Oceanic and Atmospheric Administration
Grant Numbers NA81RAH00001 and NA85RAH05045

Cooperative Institute for Research in the Atmosphere
Colorado State University
Foothills Campus
Fort Collins, CO 80523

August, 1986

Colorado State University

ABSTRACT

A MODELING STUDY OF VISIBILITY IN THE GRAND CANYON

Using a backward version of the Monte Carlo Radiative Transfer model, radiance values in the Grand Canyon were simulated to within the precision of ten percent. The contiguous spectral contrast was introduced to distinguish between adjacent areas of the same target and compared to the apparent spectral contrast. The contiguous spectral contrast is a valuable tool in evaluating visibility because in some cases, the target became more distinguishable when viewed against the sky while the target features became less distinguishable. Average equilibrium radiance values were calculated and incorporated into the Koschmieder estimate; the Koschmieder estimate was deemed to be of limited value in the Grand Canyon because of the violation of the assumptions used to derive the estimate.

It was shown that first order scattering results alone could be used to estimate apparent spectral contrast to within a 10% accuracy; higher order scattering must be considered when radiance values are calculated for the Grand Canyon scene.

Michael Jeffrey Weissbluth
Atmospheric Science Department
Colorado State University
Fort Collins, CO 80523
Fall 1985

ACKNOWLEDGEMENTS

I am happy to express my sincere gratitude and thanks to several people who made significant contributions to this research effort. Dr. Stephen K. Cox provided invaluable encouragement and guidance as my adviser. Dr. Thomas B. McKee lended support and important suggestions. I also wish to thank Dr. John M. Davis during the many consultations on the use and application of the Monte Carlo Radiative Transfer model. Thanks are due to Ms. Judy Sorbie for the expert drafting of the figures. Finally, special thanks to Ms. Melissa Tucker for her patience and cheerfulness in the preparation of numerous drafts and the final version of this manuscript.

This research was sponsored in part by the National Oceanographic and Atmospheric Administration and the National Parks Service through grant number NA81RAH00001 and NA85RAH05045.

TABLE OF CONTENTS

LIST OF TABLES

LIST OF TABLES, (Continued)

LIST OF FIGURES

LIST OF FIGURES, (Continued)

I. INTRODUCTION

Visibility is widely known to be adversely affected by aerosols in the atmosphere. While pollutants may be most concentrated in urban areas and industrialized sites, they are dispersed by local and synoptic weather systems and find their way into the pristine areas of our national parks. In areas such as the Grand Canyon, visibility can also be adversely affected by particles which are physically broken from the surface. Relatively low concentrations of these so-called dispersion nuclei and aerosol pollutants will degrade the scenic quality of distant features, while higher concentrations will make these features indistinguishable from the background.

In order to quantify visibility, the inherent spectral radiance and the apparent spectral contrast will be used (Malm, 1979). The inherent spectral radiance of a target refers to the hypothetical concept of an instrument located at zero distance from the target measuring the target's radiance. This is opposed to the apparent spectral radiance which is the radiance value observed at some distance from the target and includes the residual image-forming light from the target and the path radiance due to scattering processes throughout the path. The apparent spectral contrast will allow a comparison between the apparent spectral radiance values from the target and the sky.

The strength of the apparent spectral contrast rests in its ability to distinguish between a scene and the background. However, some way is needed to distinguish between features in the scene, and to this end,

the contiguous spectral contrast is introduced. Defined in an analogous way to the apparent spectral contrast, the contiguous spectral contrast will allow us to examine how the aerosol affects the detail of the target.

While aerosol concentration plays an obvious role in affecting visibility, sun geometry, viewer position, target reflectance, foreground reflectance and scene geometry also play critical roles in degrading or enhancing visibility. The Grand Canyon is well suited to model since it is a natural trap for aerosols and because the above variables can be manipulated in a depiction of the Grand Canyon. The depiction can be created by approximating the scene with a series of three-dimensional rectangles which can then be incorporated into a backward Monte Carlo Radiative Transfer model to quantitatively determine the importance of the above variables.

The variability or noise of the Monte Carlo radiative transfer model used to simulate the Grand Canyon scene will be investigated to determine the number of photons needed to resolve target radiances to within ten percent. The radiances for targets in a Rayleigh atmosphere and an aerosol atmosphere will be calculated at varying distances and reflectivities to determine the physical effects of an aerosol atmosphere upon target radiances. In addition, apparent spectral contrast and contiguous spectral contrast values will be examined as functions of foreground reflectance and observer position.

The variation of sky radiances with viewer azimuth angle under theoretical and typical sun geometries will also be investigated. Using data from the computations of these equilibrium radiance, the apparent and contiguous spectral contrasts derived from a single order scatter

model and multiple order scatter model will be compared. An attempt will be made to parameterize these equilibrium radiances so that they may be used in determining the validity of the Koschmieder estimate. The Koschmieder estimate relates the apparent radiance of a target to a transmission term and a scattering term. Each assumption used to derive the Koschmieder estimate will be examined to determine its importance relative to the Grand Canyon model. Finally, apparent and contiguous spectral contrasts determined from the Koschmieder estimate will be compared to those determined from the Monte Carlo radiative transfer model.

II. METHODS

The following chapter will describe the specifics of the scene depiction of the Grand Canyon. A continental aerosol is introduced into the model for several sun-scene-observer geometries. The size distribution of the aerosol used in the model is compared against one actually observed in the Grand Canyon, and its phase function is presented. Mathematical definitions for apparent and contiguous spectral contrasts are given, as well as a formula to equate the two. Koschmieder's equation and the three assumptions used to derive it are presented. The concept of equilibrium radiance is also discussed.

2.1 The Scene

The Grand Canyon scene was developed by approximating features depicted in a photograph of the scene, (see figure 1a), with increasingly course rectangles until a manageable grid emerged that could be stored in a computer. The goal was to recreate the fundamentals of the scene and not necessarily the scene itself. A small computer program was written to determine the target heights and distances from the observer taking into account the earth's curvature. The result was a 10 x 13 grid in the horizontal and a 17 layer grid in the vertical extending to 15 km. Of these 17 levels, 7 of them were required to describe the actual Grand Canyon scene. The final scene is delineated in figures 1b and 1c, which shows the modelling effort in perspective and in a plane view, respectively. The 3-dimensional rectangles of the grid were either defined as canyon features,

Figure 1a. Photograph of the Grand Canyon scene.

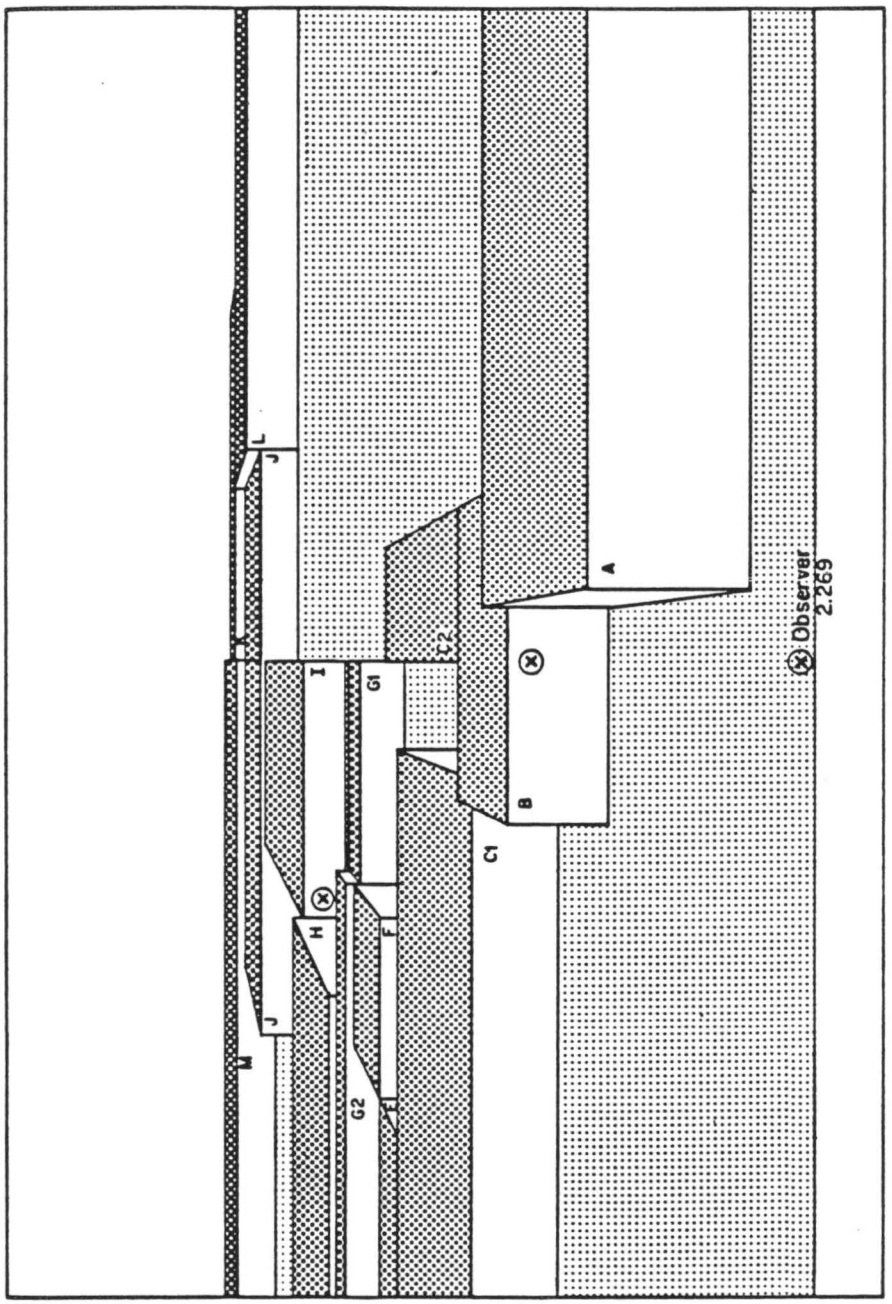

Figure 1b. Perspective view of the Grand Canyon model. The areas of targets 'I' and 'B' that are viewed by the observer are indicated by a circled X.

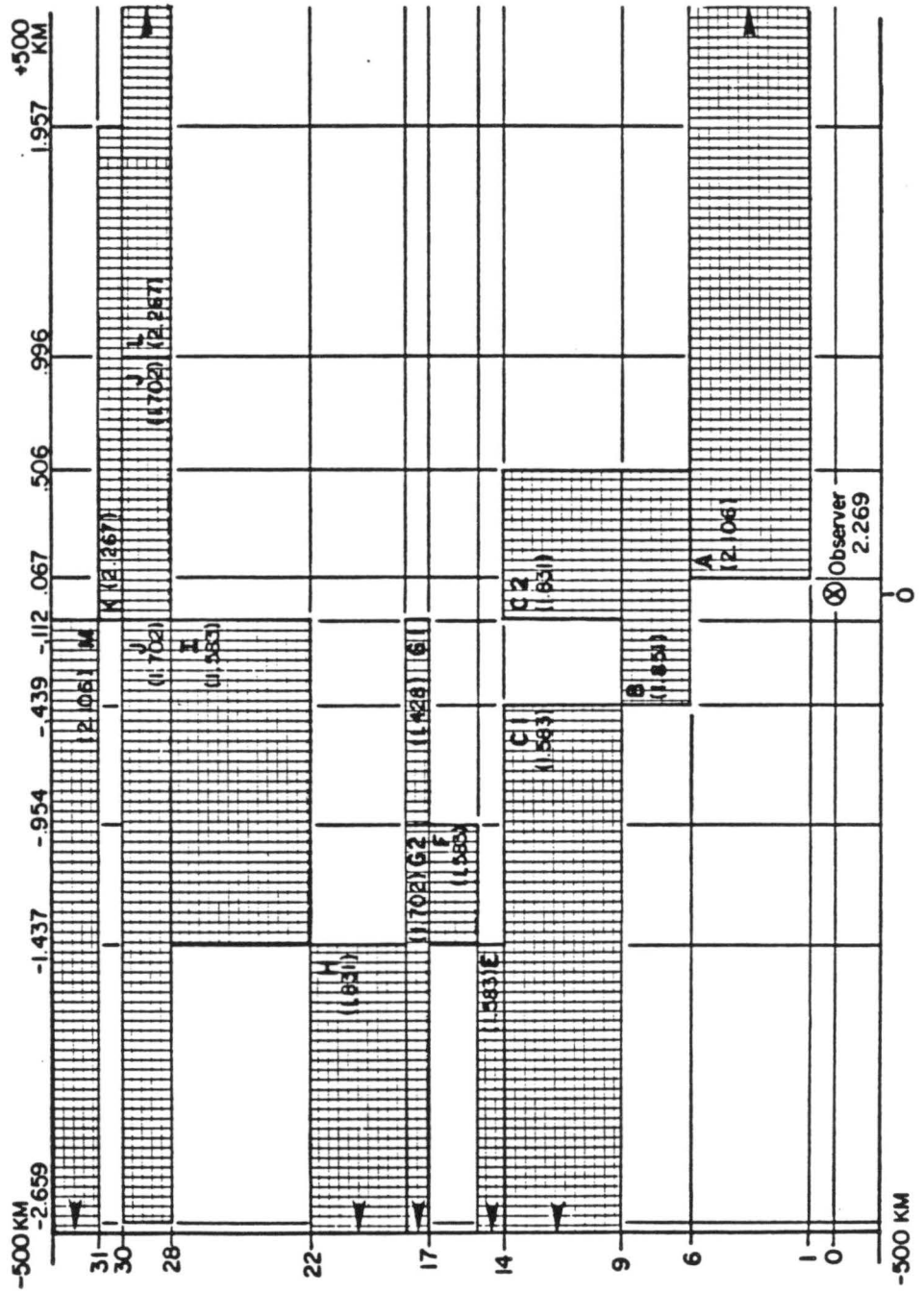

Figure 1c. Planar view of the Grand Canyon model

foreground, or air. These air boxes were designated as either a Rayleigh or clear-air box, or as an aerosol plus Rayleigh box. The distinction between the foreground and canyon features was made so that the reflectance of each could be manipulated separately.

The aerosol dispersion considered here was taken an optical boundary layer model of Elterman (1970), where the number density of the aerosol is exponentially decreased with height in the atmosphere according to a simple scale height algorithm. The aerosol number densities in the remaining ten kilometers of the atmosphere are proportional to those of the U.S. Standard Mid-Latitude Winter Atmosphere of 1962 given by McClatchey et al., (1971). The algorithm used here forces an aerosol plus Rayleigh extinction coefficient of 0.012 km^{-1} at a height of five kilometers if the extinction coefficient is 0.047 km^{-1} at the ground which in the model is set 0.5 kilometers above sea level. If we consider only conservative scattering, this implies an aerosol scattering coefficient of 0.005 km^{-1} at five kilometers and 0.036 km^{-1} at the ground. The aerosol plus Rayleigh extinction coefficient at the observer height of 2.269 km is 0.026 km^{-1}.

Solar geometry can also be altered and several different azimuth/zenith angles were used to simulate actual afternoon and morning conditions, and to do comparison studies of adjacent shadowed and lighted features of the Grand Canyon. We will refer to a sun zenith of 69.033° and an azimuth of -194.534° as 'theory left' since the sun is over the left shoulder of an observer and a sun zenith of 72.827° and an azimuth of -177.000° as 'theory right' since the sun is over the right shoulder of an observer. In addition, the 'morning' case refers to a sun zenith of 76.30° and azimuth of -34.76° and is representative of the

sun geometry at this particular scene in the Grand Canyon at 9:00 AM on 30 November. The 'afternoon' case is representative of conditions at 3:00 PM on 30 November and refers to a sun zenith of 68.02° and an azimuth of -121.57°. A sketch of the observer-sun-scene geometry as well as a summary of the sun angles used are included in figure 2.

Apparent spectral contrast (C_r), as defined by [N-N(0)]/N(0), where N is the radiance value detected by viewing a specific feature and N(0) is a background radiance, is a convenient way to quantify visibility at a distinct wavelength of radiation. A discussion of the nature of the apparent spectral contrast as it affects visibility may be found in Malm (1979) and Duntley et al. (1957). Note that the spectral contrast described here and in Duntley et al. is evaluated at a single wavelength and that this is different than the psycho-physical contrast which is the integral of the spectral contrast weighted by the photopic response curve of the unaided eye. The value of the apparent spectral contrast indicates how well a detector at a given wavelength can resolve some feature against the background. For example, a value of $|0.02|$ is often taken as the magnitude below which an object is no longer distinguishable from the background. The value of the apparent spectral contrast is of course affected by the geometry of the problem, the amount and nature of the intervening medium, the wavelength of the radiant energy and the values of the surface reflectances.

In order to fully investigate an aerosol's effect upon visibility, the contiguous spectral contrast (C_c) will be introduced. Defined as [N(light)-N(dark)]/N(light), where N(light) and N(dark) are the radiance values detected by viewing the lighter and darker portions of the same target, the contiguous spectral contrast will allow us to quantify how

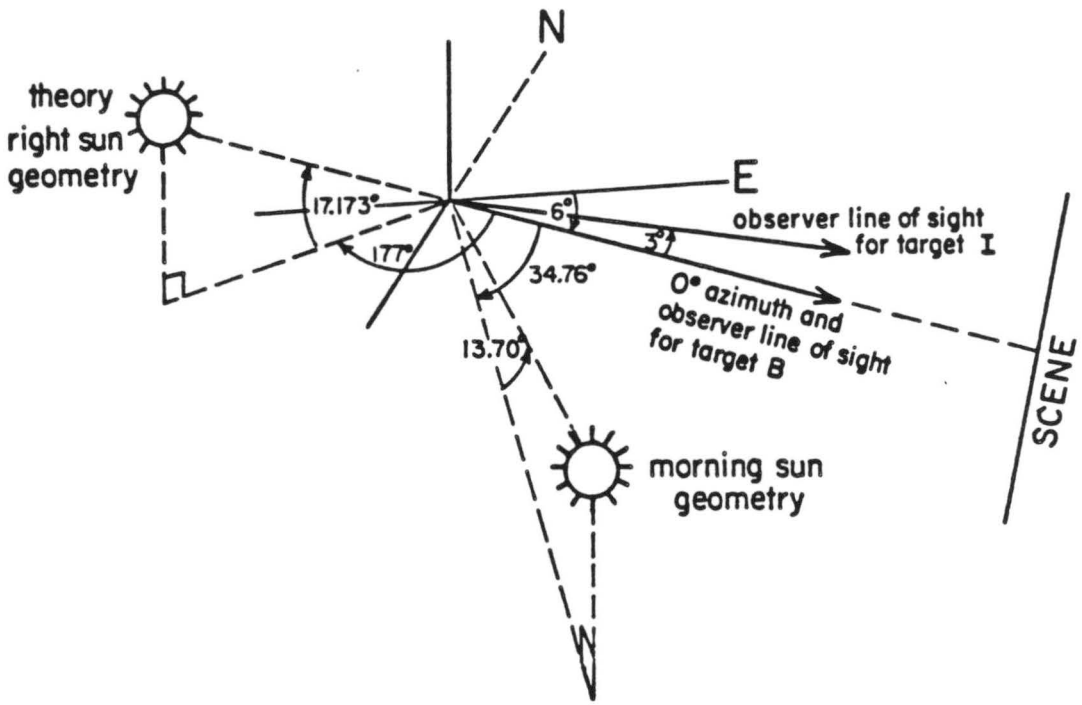

sun geometry	sun azimuth angle	sun zenith angle
morning 9:00AM 30NOV	-34.76°	76.30°
afternoon 3:00PM 30 NOV	-121.57°	68.02°
Theory Right	-177.00°	72.827°
Theory Left	-194.534°	69.033°

Figure 2. Summary of the scene geometry and the solar angles used

well an observer can view the detail of a target. In this study, N(light) will refer to the illuminated portion of the target and N(dark) will refer to a contiguous shadowed portion of the same target. If the apparent spectral contrasts are available for adjacent areas of the same target, then using the definitions presented previously for C_c and C_r the contiguous spectral contrast and the apparent spectral contrast are related by the expression:

$$C_c = [C_r(ill) - C_r(shad)] / [C_r(ill) + 1].$$

The value of the contiguous spectral contrast will vary between zero, which indicates no distinction between the adjacent areas of the target, and one, which indicates a very sharp distinction between the adjacent areas. Note that in this study, the contiguous spectral contrast cannot assume negative values as can the apparent spectral contrast.

2.2 The Radiative Transfer Model

Radiances were determined by using a backward Monte Carlo Radiative Transfer model similar to that described by Collins et al. (1972) for a spherical shell atmosphere. The backward model traces the photon's path from the observer to the top of the atmosphere. It is considerably more efficient than the forward version of the model because each photon that is traced by this program will contribute to the radiance along the particular line of sight of interest. Radiances from the model are relative to an incident irradiance of π. Therefore, all radiances presented here are dimensionless.

Several important parameters need to be specified when using the Monte Carlo method. A wavelength of 0.55 microns was used for all runs of the model. A Deirmendjian (1969) Haze L continental haze aerosol

distribution was used. The Haze L model obeys a modified gamma distribution and has a modal radius of 0.07 microns. Measurements of a Grand Canyon aerosol (Malm, personal communication) indicate a modal radius of 0.09 microns and a log normal distribution. Figure 3 shows the differences in the distributions when the number concentration is plotted against the radius. It is interesting to note that the modal radius of the log-normal distribution does not appear at 0.09 microns when plotted in this fashion. It would, however, appear at 0.09 microns if the log of the number distribution were plotted. The Haze L distribution, while not conforming to the observations exactly, allows the use of a recognizable model to simulate the important characteristics of the aerosol. Throughout the visible spectrum, the single particle scattering albedo of the Haze L model was set to unity, indicating no absorption of radiation by the aerosol being considered.

Either a Rayleigh atmosphere or a Rayleigh plus aerosol atmosphere, hereafter referred to as an aerosol atmosphere, was used for the model calculations. In the Rayleigh case, the phase function is representative of forward and back scattering of equal intensity, while in the aerosol plus Rayleigh case, the composite phase function is representative of strong forward scattering, as shown in figure 4. Although the phase function is usually displayed upon polar graph paper, one half of the phase function is plotted on linear graph paper to capture the salient features. The remaining half of the phase function can be easily deduced by recognizing that it must be symmetrical. By comparing the Rayleigh and aerosol model results, the aerosol's effects on visibility can be deduced.

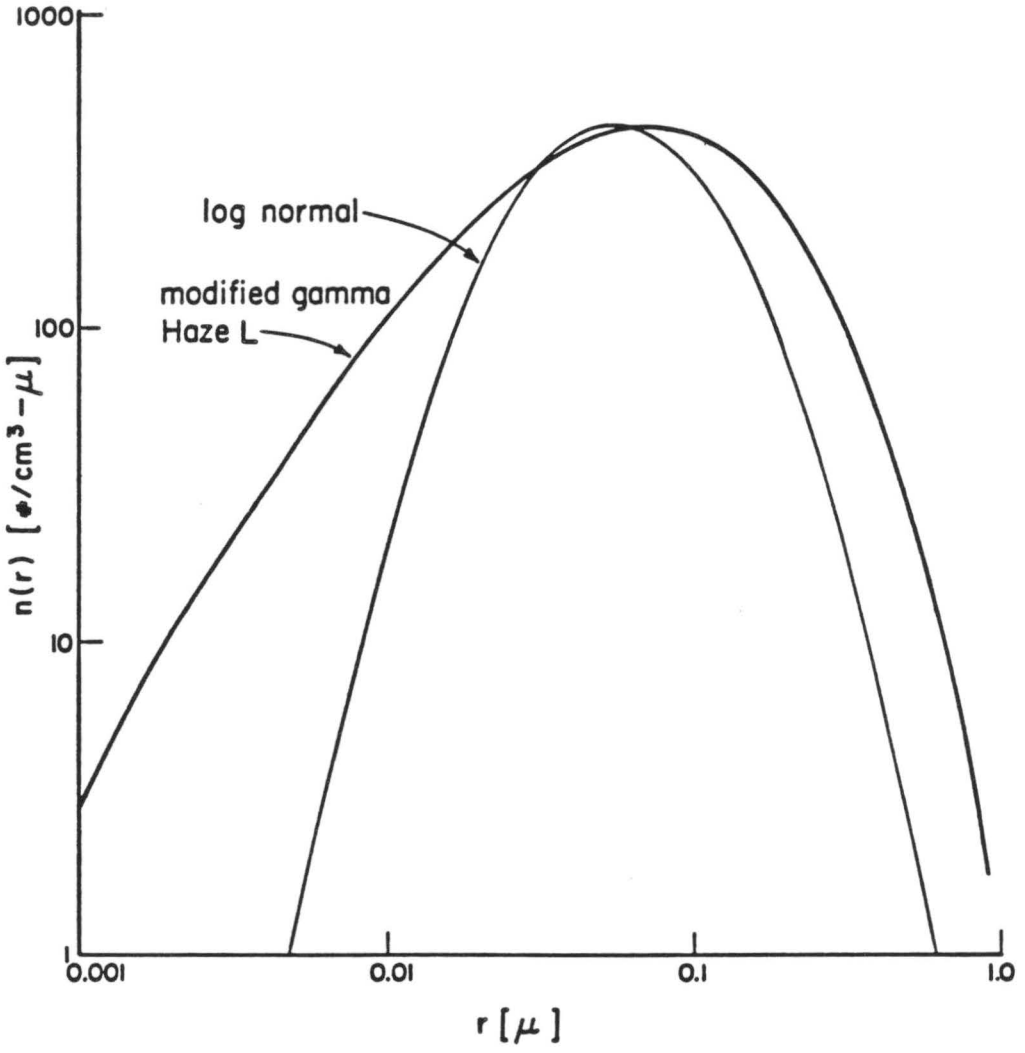

Figure 3. Comparison of the modified gamma number distribution used in this study and the log normal number distribution

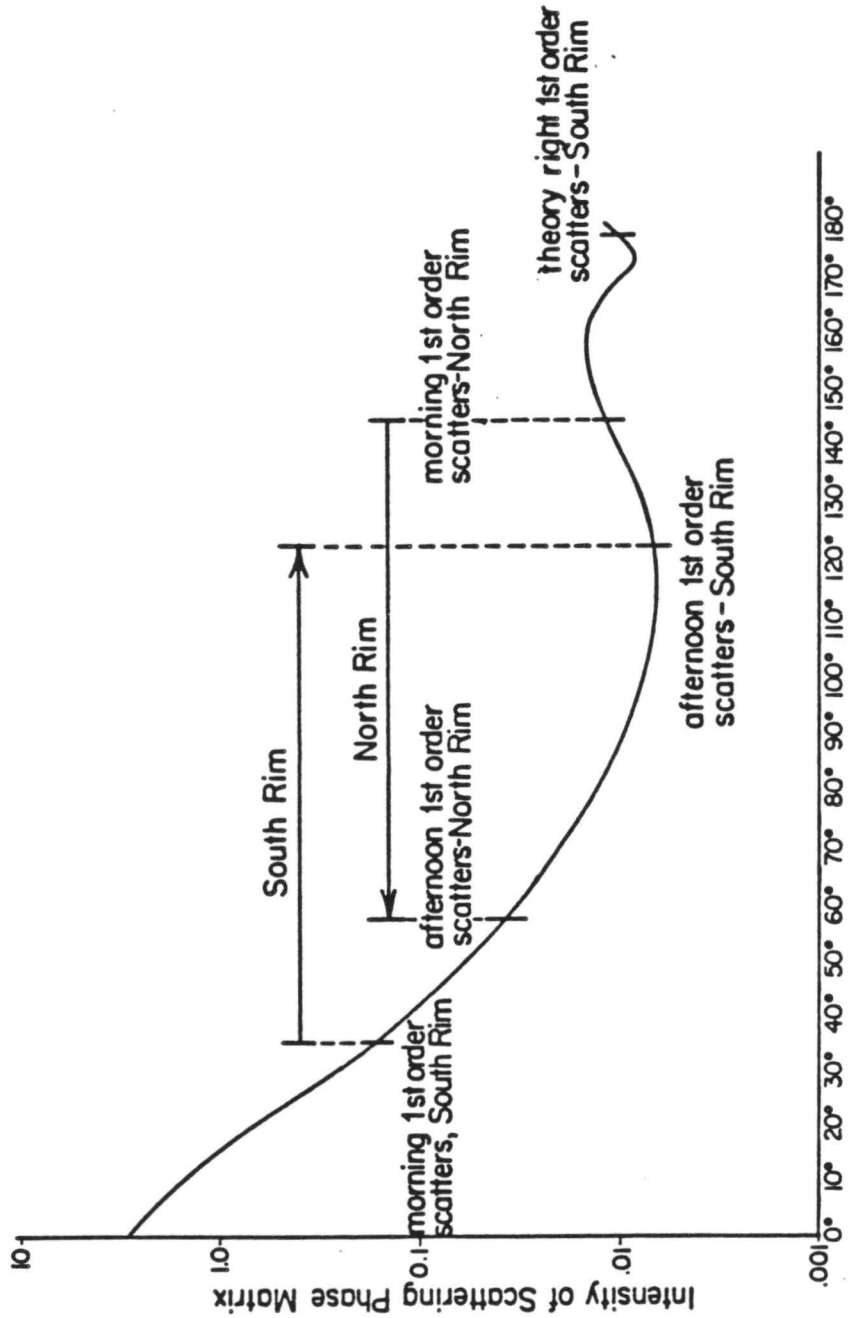

Figure 4. Aerosol phase function used in this study with indications where first order scatter events would occur using various solar geometries.

The target reflectance can also be changed in the model to see its effect on visibility. Assuming that the mountains behave as a Lambertian reflector, an albedo of 0.15 is appropriate for bare rock while 0.75 is appropriate for a snow covered surface. The reflectance of surface features, however, is accurately represented only by a bidirectional reflectance pattern. A bidirectional reflectance model was selected from Davis and Cox (1982) for the Saudi Arabian desert to investigate the importance of variation in target reflectance. The desert was chosen because of the similarity in color to the Grand Canyon rock and because data were available. The desert model indicates that variations in surface reflectances as an observer scans through ten degrees of azimuth are less than ten percent. This variation is less than the variability of the model and was thus judged to be insignificant. It should be noted, however, that the Grand Canyon model is composed of plane parallel surfaces which probably don't show a large variation in reflectance. The actual scene, of course, is comprised of many variously oriented targets whose faces, which show large angular variation in orientation, may behave as specular reflectors as well as Lambertian reflectors. Therefore, the fine details of the Grand Canyon are not captured by this rather simple model.

2.3 Koschmieder's Equation

Another area that will be explored is the approximation of calculated radiances by the Koschmieder equation. Preisendorfer (1976) reviewed Koschmieder's study of the problem of the apparent radiance of an object as seen along a path of sight. Koschmieder's equation employs three fairly restrictive assumptions: 1) the path lies in a homogeneous and uniformly illuminated region, 2) the path is horizontal so that the

extinction coefficient is not a function of height, and 3) the radiance distribution is independent of height along the path. From these assumptions, the following simple analytic expression emerges from the radiative transfer equation for the radiance:

$$N = N(0)\exp\{-br\} + N(q)[1-\exp\{-br\}].$$

The quantity br represents the optical depth of the medium with r representing the path length and b representing the extinction coefficient, N is the radiance as seen by the observer, N(0) is the radiance reflected by the target at r = 0, and N(q) is the equilibrium radiance.

The significance of the equilibrium radiance can be seen by setting r to infinity in the above equation. In this case, the radiance as seen by the observer is equal to the equilibrium radiance. Therefore, in order for the target radiance to approach the equilibrium radiance as the observer-target distance increases, we can conclude that targets brighter than this equilibrium radiance will appear darker as the observer moves away, and targets that are darker than this equilibrium radiance will appear brighter as the observer moves away. In this particular study, the equilibrium radiance was determined by viewing along a particular line of sight with only the atmosphere present.

III. RESULTS AND DISCUSSION

This chapter will explore the variability inherent within the Monte Carlo radiative transfer model and determine the number of photons needed to characterize the apparent spectral radiance of the target to within ten percent. Target radiances will then be explored as a function of target reflectivity to determine the aerosol's effect upon visibility. In addition, target radiances will be explored as a function of foreground reflectance and observer position to determine the aerosol's effects upon the apparent and contiguous spectral contrasts. Equilibrium radiance values are then calculated by removing all features from the canyon and these values are paramaterized. In addition, apparent and contiguous spectral contrasts derived from a single order scatter model and a multiple scatter order model are compared. The Koschmieder estimate is then examined in the context of the three assumptions used to derive it. Finally, the apparent and contiguous spectral contrasts derived from the Koschmieder equation and the Monte Carlo model are compared.

3.1. Model Variability

Variability of the model was tested for a featureless canyon using the morning geometry. The observer's line of sight varied in degree increments from five degrees left to five degrees right of zero degrees azimuth. Four Monte Carlo computer runs of 800 photons each were used in examining the variability of the model with a ground reflectance of

0.1 and the results are shown in table 1. The standard deviation defined as:

$$SD = [(\Sigma X_i^2 - n*(mean))/(n - 1)]^{1/2},$$

where the summation over i goes from 1 to n is used as a measure of variability of the model. The standard deviation ([SD]) indicated in the table is bracketed because only four samples were used for its determination and thus n is small. Similarly, the coefficient of variation ([COV]), which was found by dividing the standard deviation into the mean, is also bracketed. Although using only four samples is not statistically sound, it does provide a measure of the variability of the model. In order to determine the true standard deviation and coefficient of variation, three consecutive observer azimuth angles centered about zero degrees azimuth and consisting of four 800 photon model runs each were used (n=12). The mean was 0.3933 and the SD was 0.0206 producing a COV of 5.2 %. Therefore, 800 photons was judged sufficient to characterize sky radiances to within five percent in a featureless canyon. If we look at the [COV] row in table 1, we see that most of the coefficients of variation are about five percent, with one being as high as ten percent and another being as low as two percent. Therefore, using only four runs to determine the [COV] provides an indication that the true COV can vary from between one-half and two-times the [COV].

TABLE 1

Morning simulation case for a featureless canyon
using 800 photons/line of sight

	OBSERVER AZIMUTH ANGLE									
	5°	4°	3°	2°	1°	0°	-1°	-2°	-3°	-4°
run number										
1	.3682	.3008	.3684	.3817	.3826	.3896	.4193	.4523	.4623	.5110
2	.3233	.3200	.3713	.3955	.3870	.4155	.3613	.4310	.4474	.4542
3	.3669	.3438	.3572	.3952	.3688	.3790	.3967	.4342	.4224	.4601
4	.3914	.3855	.3250	.4167	.3928	.3954	.4317	.4372	.4528	.4533
mean	.3625	.3375	.3555	.3973	.3828	.3949	.4023	.4387	.4462	.4697
[SD]	.0284	.0365	.0212	.0145	.0102	.0153	.0309	.0094	.0170	.0277
[COV]	7.8 %	10.8 %	6.0 %	3.6 %	2.7 %	3.9 %	7.7 %	2.2 %	3.8 %	5.9 %
aver		.3518	.3634	.3785	.3917	.3933	.4120	.4291	.4515	

Variability of the model for a canyon depiction including targets for two solar geometries was determined by calculating the radiances for 200 photons or 800 photons in four different Monte Carlo computer runs. The results for the 800 photon runs for the morning case, shown in table 2, indicate that the largest [COV] in the model occur with the closest targets. Because the [COV] is determine by dividing the [SD] into the mean, targets with low mean radiances will be expected to have fairly high coefficients of variation. Although target 'A' has an unacceptably high [COV], all other targets have [COV]'s on the order of ten percent.

We would then expect the true COV to be as low as five percent and as high as twenty percent. Since the SD and thus the COV will decrease with the square of the number of observations, 3200 photons was judged sufficient to represent target radiances to within ten percent when the target was farther than six kilometers away from the observer in the morning geometry .

As targets move further away from the observer, the [SD] increases due to the increased probability of the photon's path between the observer and target being altered by a scattering event. This is illustrated in table 2, as well as in the Sky case of table 3, where the [SD] increases as the target distance increases. In the Sky case, all features were removed from the canyon model and a Rayleigh atmosphere was used. Then a minimum of scattering events occured between the photons and the sky and target and we would expect a very low [SD].

TABLE 2

Morning simulation case using 800 photons/line of sight

	FEATURE			
run number	A(1 km)	B(6 km)	I(22 km)	K(30 km)
1	0.007594	0.02118	0.1334	0.1876
2	0.01211	0.02197	0.1434	0.2245
3	0.008980	0.02080	0.1492	0.1976
4	0.01105	0.02684	0.1509	0.2081
mean	0.009934	0.02268	0.1442	0.2045
[SD]	0.0020	0.0028	0.0079	0.0158
[COV]	20.4 %	12.4 %	5.5 %	7.7 %

Results of four 200 photon runs using a theory right solar geometry (see figure 2) are shown in table 3. Since the [COV]'s are all below ten percent, 200 photons would produce true COV's between five and twenty percent. Therefore, 800 photons were judged sufficient to characterize the target's radiance with the sun in a theory right or theory left geometry. In addition, 800 photons was judged sufficient in an afternoon solar geometry because of the nature of the aerosol phase function. Figure 4 shows the Haze L aerosol phase function, and the portions where first order scatters occur in the theory right and afternoon solar geometries. Because both occur in a slowly changing area of the phase function, we would expect both solar geometries to

produce similar coefficients of variation. Also, because the sky line of sight has such a low [COV], 200 photons was judged sufficient to represent the sky radiances of a featureless canyon for the theory right, theory left, and afternoon solar geometries.

TABLE 3

Theory right simulation case using 200 photons/line of sight

	FEATURE				
run number	A(1 km)	B(6 km)	I(22 km)	K(30 km)	Sky
1	0.06260	0.06578	0.1247	0.1226	0.3212
2	0.06438	0.06974	0.1081	0.1298	0.3197
3	0.06493	0.05810	0.1043	0.1341	0.3229
4	0.05956	0.06621	0.1247	0.1524	0.3206
mean	0.06287	0.06496	0.1155	0.1347	0.3211
[SD]	0.00242	0.00490	0.01097	0.00235	0.0013
[COV]	3.8 %	7.5 %	9.3 %	1.7 %	0.42 %

3.2.0 Radiance Computations

Sky radiances over target 'B' were computed with the sun in front of the observer and behind the observer and are shown in figure 5. The similarity of the slopes prompted an investigation into the variability of the slope of a line passing through data points which themselves were derived from several computer runs and thus represented a mean with a certain standard deviation. Pseudo-random numbers were generated which had a 3.9 % standard deviation about the mean as the model variability studies indicated in table 3 for an azimuth viewing angle of zero degrees. The results indicated that the slopes of the lines were identical given the 3.9 % uncertainty in the model generated radiances. Furthermore, slopes of lines which appear similar can statitistically be called equal since the model generated radiances show variations of at least 3.9 %.

3.2.1 Target Reflectance

Radiances as a function of the target reflectance were calculated for targets 'B' and 'I' (see figure 2), respectively six and twenty-two kilometers away from the observer. Sun angles used were theory left for target 'I' and theory right for target 'B', which places the sun over the observer's left and right shoulder, respectively. Figure 6 shows the results for the target six kilometers away while figure 7 shows the results for the target twenty-two kilometers away. Immediately apparent is the similar behavior of the illuminated portions of both graphs and the shadowed portion, reinforcing the intuitive notion that increasing the reflectance of an object will make it significantly brighter only if the object is in direct sunlight. The shadowed areas of both targets are less sensitive to the change in reflectance because only photons

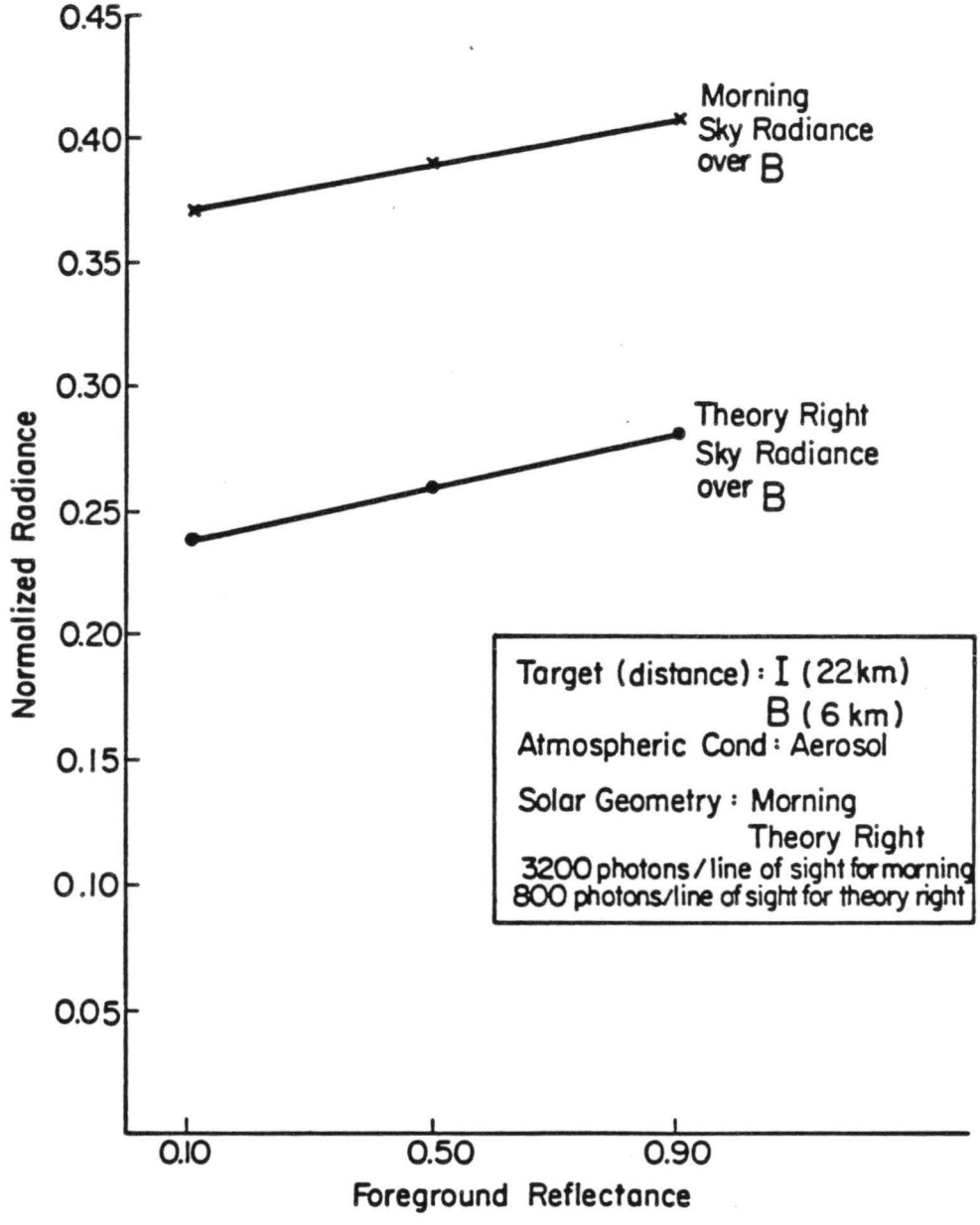

Figure 5. Radiance values plotted as a function of foreground reflectance for sky radiances over target 'B'

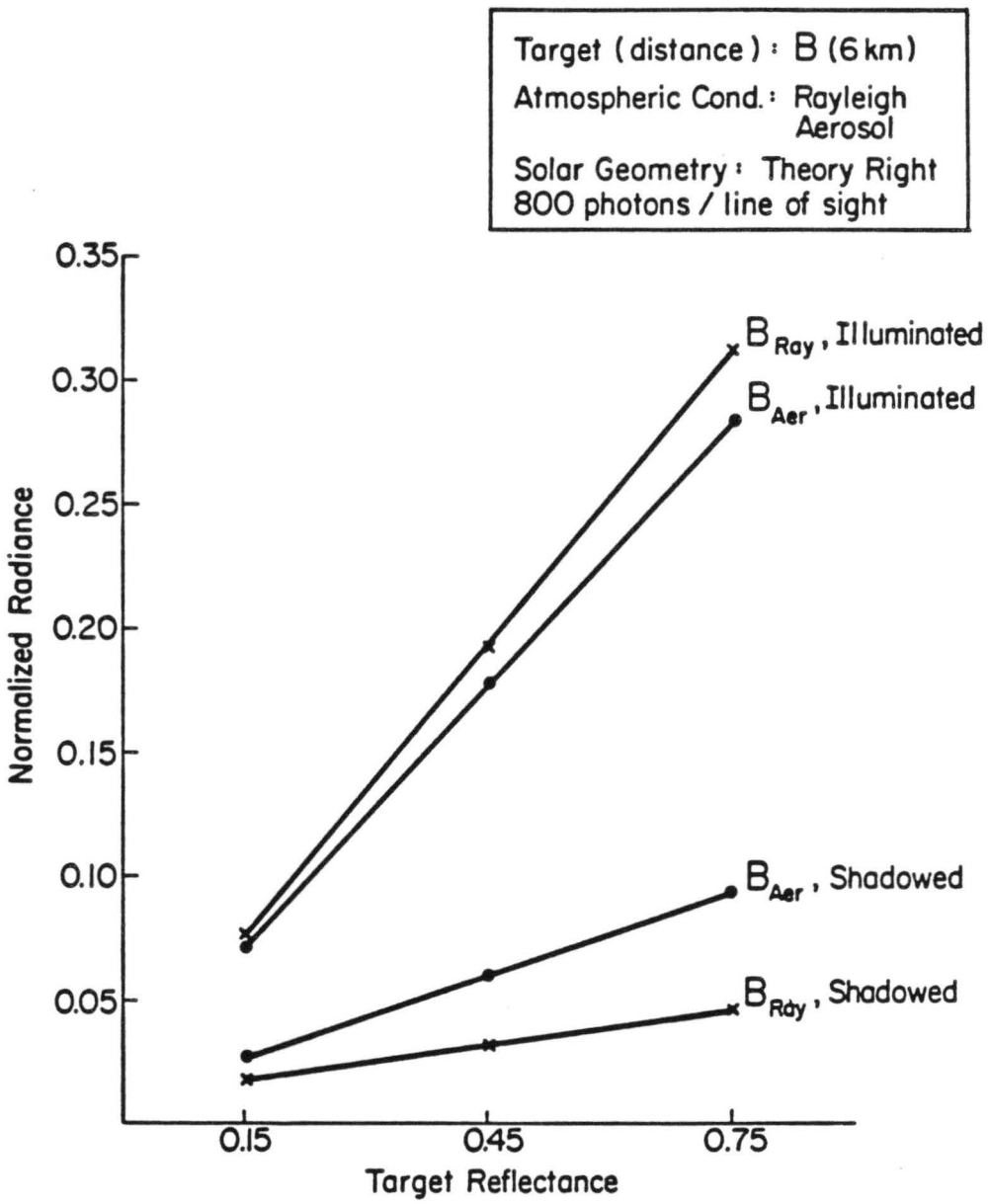

Figure 6. Radiance values plotted as a function of target reflectance for target 'B' using a Rayleigh and aerosol atmosphere

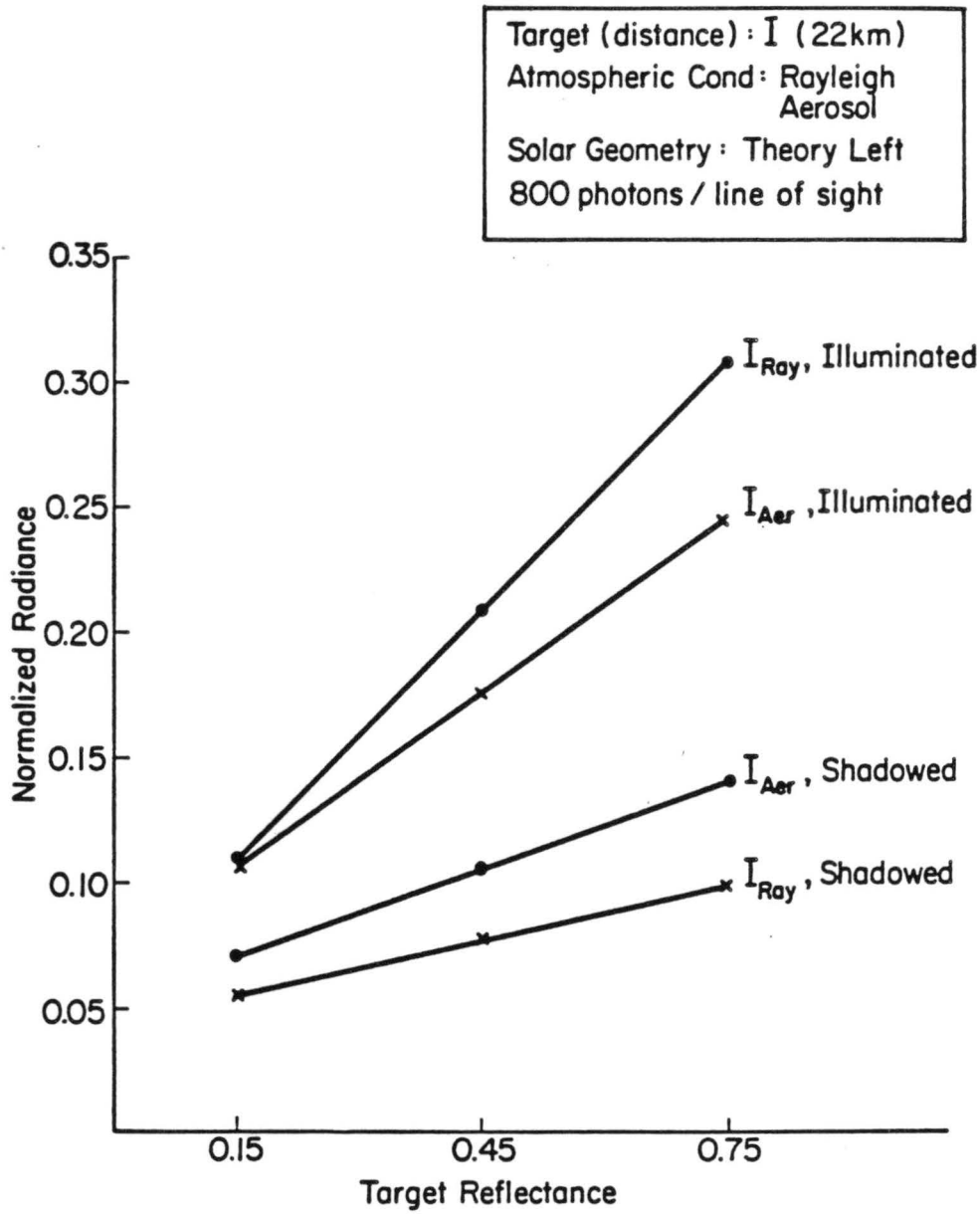

Figure 7. Radiance values plotted as a function of target reflectance for target 'I' using a Rayleigh and aerosol atmosphere

which will have first undergone at least a first order scatter will be reflected from the target.

Of further interest are the slopes of the curves for each target. The Rayleigh and aerosol curves for the illuminated portion of target B are nearly identical in slope, while the Rayleigh curve is significantly steeper in slope than the aerosol curve for the illuminated portion of target I. This can be explained by considering the offsetting effects between the aerosol's scattering characteristics and the increased target reflectance. Although the inherent radiance of the target increases due to its increased reflectance, the aerosol depletes this increased radiance by scattering photons out of the line of sight of the observer. The increased radiance of the near target from its increased reflectance is not depleted by the aerosol as much as the far target because the path length is shorter and the optical depth is thus correspondingly smaller.

The addition of path light by both the Rayleigh and aerosol atmospheres can be seen by comparing the radiance values for the shadowed portion of both targets. The radiance values for the shadowed portion of target I are nearly twice as high as the radiance values for the shadowed portion of target B. This is because the path length for target I is longer, thus allowing the addition of more path light to the inherent radiance of the target by the atmosphere.

By comparing the illuminated regions of targets I and B for the aerosol case and the Rayleigh case, we find that at smaller target reflectances, the atmosphere will add path light to and thus enhance the inherent target radiances, while at larger target reflectances, the atmosphere will deplete the inherent target radiances. Furthermore,

this reversal occurs at higher target reflectances for the Rayleigh case than for the aerosol case. The radiance value where the atmosphere neither enhances or depletes the inherent target radiance is referred to as the equilibrium radiance. The concept of equilibrium radiance will be elaborated upon later in section 3.3.

3.2.2 Foreground Reflectance

Also of considerable importance is the effect of foreground reflectance upon target radiance. Theory left and theory right cases were used to capture the light-dark contrasts of the target while emulating the backward scattering characteristics of the aerosol. The morning case was used so that the forward scattering characteristics of the aerosol could also be examined. Figure 8 shows the aerosol cases and Rayleigh cases for targets 'I' and 'B' in the morning. Immediately apparent are the higher target radiances for the aerosol atmosphere which arise from the forward scattering characteristics of the aerosol. The similar slopes of the aerosol and Rayleigh curves can be explained by considering the foreground as providing additional illumination from the bottom of the scene. The apparent target radiance will then increase regardless of whether the observer is viewing the target in a Rayleigh of aerosol atmosphere.

Figure 9 shows the results of the calculations for the theory left and theory right configurations. The shadowed and illuminated curves for target B and I are nearly parallel, indicating that an equal number of photons are reflected from the illuminated and shadowed portions of the target and that there is an equal addition of path light from the aerosol to both areas of the target. Therefore, there is no significant

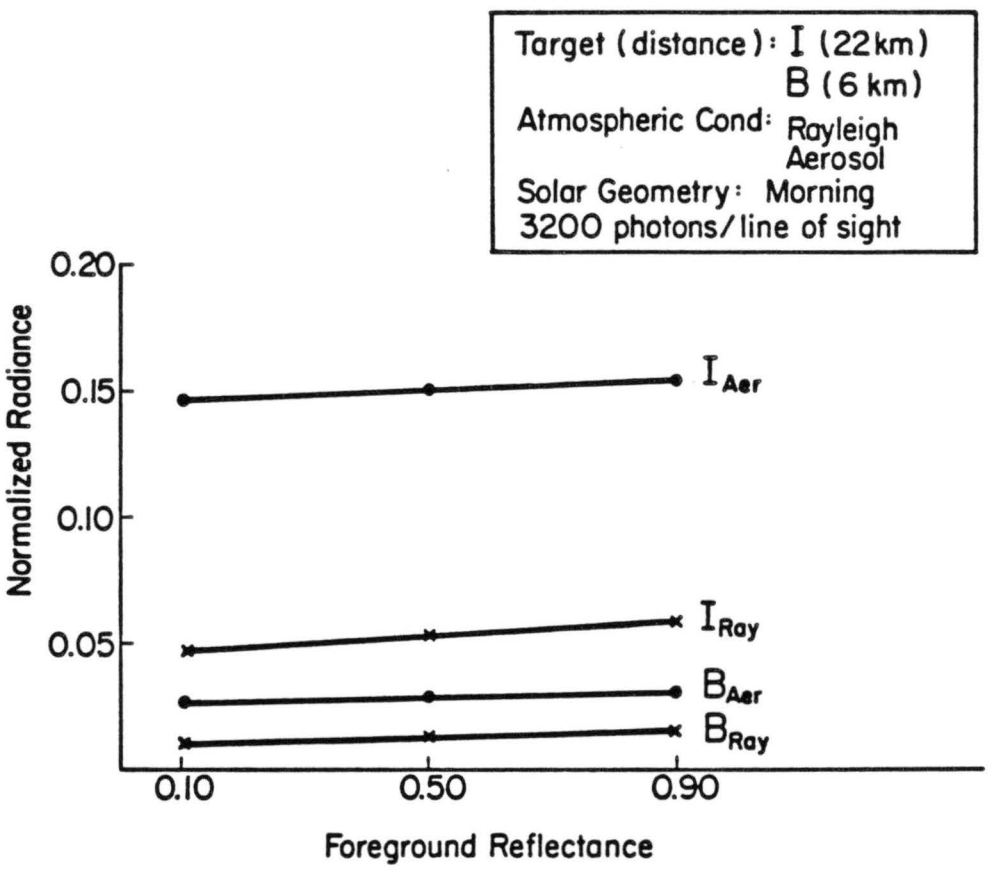

Figure 8. Radiance values plotted as a function of foreground reflectance for targets 'I' and 'B' using a Rayleigh and aerosol atmosphere

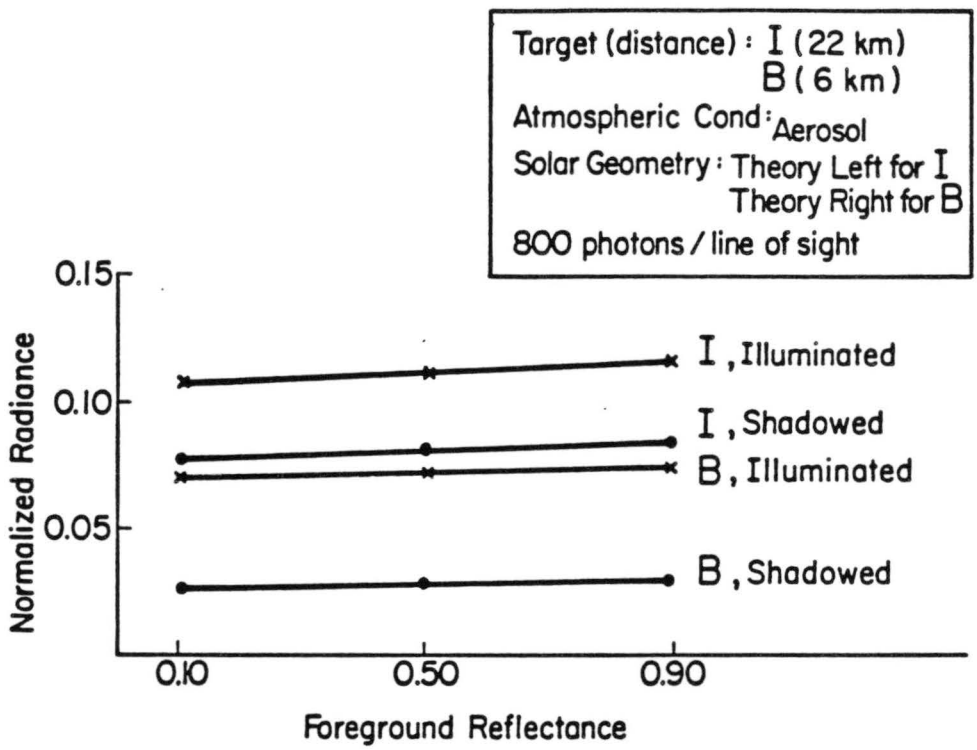

Figure 9. Radiance values plotted as a function of foreground reflectance for the shadowed and illuminated portions of targets 'I' and 'B'

change in contiguous target contrast as the foreground reflectance is increased.

Figure 10 shows the radiance calculations for the morning case with target reflectivities of 0.90 and 0.15. The relatively large radiances of shadowed targets 'I' and 'B' arise from the forward scattering characteristics of the aerosol. The 0.15 reflectance curves are very similar in slope to the theory right and theory left curves discussed above indicating the tendancy of the foreground to behave as a source of illumination. Increasing the target reflectance to 0.90 significantly increases the radiance values due to the fractionally increased number of photons reflected from the target at each scatter. The slopes are steeper because in this model, increasing the target reflectance necessarily means increasing all canyon surface reflectances. Therefore, there are a correspondingly larger number of photons being reflected onto the target from other highly reflective surfaces.

Shown in tables 4-7 are the apparent spectral contrasts for the various features. In general, the apparent spectral contrast decreases as the foreground reflectance increases because the target radiance increases proportionately faster with increasing foreground reflectance than the sky radiance does. However, the sky radiance will increase proportionately more when the line of sight passes over a large area of foreground. This is precisely what occurs in the theory right case in table 6 as the apparent spectral contrast increases with increasing foreground reflectance for target 'B'.

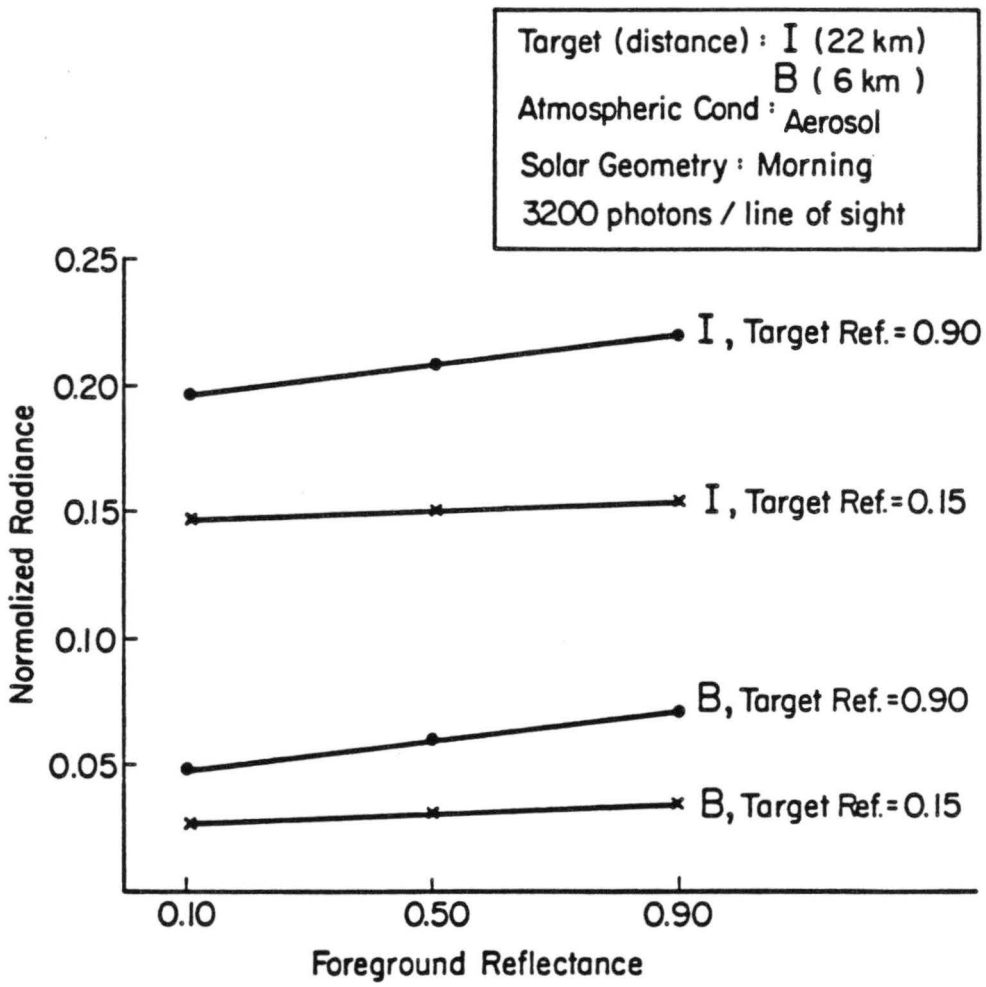

Figure 10. Radiance values plotted as a function of foreground reflectance for target reflectivities of 0.90 and 0.15 for targets 'I' and 'B'

TABLE 4

Morning sun geometry with apparent spectral contrasts
using 3200 photons/line of sight

	FEATURE			FEATURE		
gnd ref	I	sky(I)	C_r	B	sky(B)	C_r
0.1	0.1467	0.3240	-.547	0.02676	0.3716	-.928
0.5	0.1498	0.3270	-.542	0.02907	0.3876	-.925
0.9	0.1532	0.3308	-.537	0.03169	0.4079	-.922

TABLE 5

Theory left sun geometry with apparent spectral contrasts and
contiguous spectral contrasts using 800 photons/line of sight

	FEATURE			FEATURE			
gnd ref	I(light)	sky(I)	C_r	I(shadow)	sky(I)	C_r	C_c
0.1	0.1064	0.1839	-.421	0.07628	0.1839	-.585	0.283
0.5	0.1102	0.1889	-.417	0.07964	0.1889	-.578	0.277
0.9	0.1142	0.1952	-.415	0.08306	0.1952	-.574	0.273

TABLE 6

Theory right sun geometry with apparent spectral contrasts and contiguous spectral contrasts using 800 photons/line of sight

gnd ref	FEATURE B(light)	sky(B)	C_r	FEATURE B(shadow)	sky(B)	C_r	C_c
0.1	0.07091	0.2384	-.703	0.02681	0.2384	-.888	0.622
0.5	0.07263	0.2571	-.718	0.02804	0.2571	-.891	0.614
0.9	0.07439	0.2809	-.735	0.02931	0.2809	-.896	0.606

TABLE 7

Morning equilibrium radiances with apparent spectral contrasts and a target reflectivity of 1.0 using 3200 photons/line of sight

gnd ref	FEATURE I	sky(I)	C_r	FEATURE B	sky(B)	C_r
0.1	0.1953	0.3240	-.397	0.04803	0.3716	-.871
0.5	0.2072	0.3270	-.366	0.06038	0.3876	-.844
0.9	0.2195	0.3308	-.336	0.07041	0.4079	-.827

Although we have seen in table 6 that apparent spectral contrasts increase with increasing foreground reflectance, contiguous spectral contrasts decrease with increasing foreground reflectance. As the contiguous spectral contrast decreases, the features of the target tend to become more indistinct. This occurs because more photons are being scattered into the line of sight by the aerosol. Therefore, while the

target tends to be slightly more distinguishable from the background as foreground reflectance increases for the theory right sun geometry, the features of the target tend to be less distinguishable. Herein lies the utility of the contiguous spectral contrast.

3.2.3 Observer Position

Observer position may also play a critical role in affecting visibility, and to this end, apparent specral contrasts were computed for two targets for an observer positioned on the north rim of the canyon for the morning and afternoon solar geometries. The observer was placed two meters above feature 'M' and viewed target 'H', the near feature, eight kilometers away and target 'C2', the far feature, seventeen kilometers away. The results, shown in table 8, generally indicate higher contrasts and thus better visibility when the scene is viewed from the south rim of the canyon.

TABLE 8

Radiances and apparent spectral contrast for observers on the north and south rim of the Grand Canyon using 800 photons/line of sight for morning cases on the north rim and afternoon cases on the south rim, and 3200 photons/line of sight for afternoon cases on the north rim and afternoon cases on the south rim.

time	FEATURE near tar	FEATURE sky rad	C_r	FEATURE far tar	FEATURE sky rad	C_r
shadowed						
N-afternoon	0.04851	0.1957	-0.752	0.1068	0.2535	-0.579
S-morning	0.02676	0.3713	-0.928	0.1467	0.3542	-0.586
S-afternoon	0.01215	0.1418	-0.914			
illuminated						
N-morning	0.06841	0.1325	-0.484	0.08482	0.1425	-0.405
S-afternoon				0.08883	0.1418	-0.374

The low apparent spectral contrasts of the near shadowed feature when viewed from the north rim are due to the relatively high target radiance of 'H'. The high target radiance can be explained straightforwardly since target 'H' when viewed from the north rim is three kilometers farther away than target 'B' when viewed from the south rim thus allowing the aerosol to scatter more photons into the line of sight of the observer. Perhaps more significant, however, are the relatively low sky radiances observed from the north rim. A low sky radiance would result in a low apparent spectral contrast because the target and sky would have similar radiance values.

The nature of the aerosol phase function forces higher sky radiances when viewed from the south rim. Marked on figure 4, which shows the composite Rayleigh-aerosol phase function, are the areas where first order scatters would occur if the observer was on either the north or south rim of the canyon. The arrows indicate the direction along the phase function that photons undergoing first order scatters would move as the sun traversed the sky through the day. For a large part of the day, photons reaching an observer on the south rim would have to undergo first order scatters nearer to the peak of the phase function than photons reaching an observer on the north rim. Therefore, for most of the day, sky radiances and thus visibility will be higher on the south rim of the canyon. This would change in the later part of the day, but the phase function flatter in that scattering regime, so that sky radiances would be closer in the afternoon for both rims of the canyon. This is evidenced by the illuminated target viewed in the afternoon from the south rim of the canyon in table 8. The apparent spectral contrasts indicate slightly better visibility when viewed from the north rim since the south rim observer is now further from the peak of the phase function than the north rim observer.

Although apparent spectral contrast is highest when the sky radiances are highest given similar target radiances, it seems counter-intuitive that visibility is better when the effects of the aerosol are maximized. Malm (1979) suggests that apparent spectral contrast ignores the effect that sun angle has on an observer's ability to see detail or inherent color in a given vista. As the sun approaches angles that are conducive to forward scattering, the path radiance will be large and detail will tend to be washed out. Apparent target

radiance will not have changed while the ability to see the target has degraded significantly. He suggests that a 'color measurement' would be sensitive to these effects. A contiguous target contrast might also be sensitive because it can distinguish the detail within the target as seen in the previous paragraphs.

To investigate the differences between the contiguous and apparent spectral contrast values, the sun was placed behind both the north rim and south rim observers. Radiance values for adjacent shadowed and illuminated areas of a near target and a far target are calculated for a north rim observer and a south rim observer. The results, shown in table 9, indicate that, in general, as the apparent spectral contrast increases, the contiguous spectral contrast also increases. However, the apparent spectral contrast for the far illuminated target is higher for the north rim observer while the contiguous spectral contrast is higher for the south rim observer. Therefore, while the target might be more discernable when viewed against the sky from the north rim, the details of the target are more discernable when viewed from the south rim. Therefore, the contiguous spectral contrast is indeed a valuable tool for evaluating visibility.

TABLE 9

Apparent spectral contrasts and contiguous spectral contrasts for a north rim and south rim observer using 800 photons/line of sight.

target	FEATURE shadowed	sky	C_r	FEATURE illuminate	sky	C_r	C_c
North-near	0.03587	0.1537	-.767	0.08200	0.1537	-.466	.563
South-near	0.02681	0.1926	-.861	0.07091	0.1926	-.63	.622
north-far	0.08434	0.1763	-.522	0.09165	0.1763	-.480	.080
south-far	0.07628	0.1812	-.579	0.1064	0.1812	-.413	.283

3.2.4 Aerosol Absorption

In all the cases examined thus far, only conservative scattering within the aerosol has been considered. Since aerosol scattering is in general non-conservative, it is important to consider the effect of particle absorption and its effect on visibility. Davis et al., (1985) has investigated aerosol absorption in the Bryce Canyon using a similar Monte Carlo model and one mountain for the scene geometry. Davis concluded that contrast does not depend upon the aerosol absorption. The absorption depletes the radiances of the sky and mountain top by an equal fraction along the distance between the observer and the vista. Additional absorption occurs along the sky-looking line of sight beyond the vista, however the transmittance of any radiative effects beyond the vista are small (less than 10%) so that additional absorption has little influence. The almost equal reduction along the two lines of sight is removed in the ratio of contrast definition.

The major role of aerosol absorption may not be to change the apparent spectral contrast, but rather to change the color of a scene by absorption of preferential regions. The infamous Denver Brown Cloud, for example may owe its color to preferential spectral absorption. In the Haze L distribution examined, absorption does not take place at wavelengths shorter than the near infra-red. However, to accurately simulate the Grand Canyon scene, complex indecis of refraction need to be known at several wavelengths so that preferential spectral absorption can be simulated.

3.3 Equilibrium Radiance

In order to investigate the validity of the Koschmieder equation, the equilibrium radiance value of the scene must be known. The value of the equilibrium radiance is found by setting r to infinity in Koschmieder's equation in section 2.3. Unfortunately, the equilibrium radiance value varies with the observer-sun geometry. Therefore, this section will attempt to parameterize the equilibrium radiances under various sun geometries so that they may be incorporated into the analysis of the Koschmieder equation.

Table 10 shows radiance values calculated as a function of target reflectivity for features 'I' and 'B' using the theory left sun geometry and an aerosol atmosphere. The larger radiances for the distant target at low reflectances are due to the contributions of path light, that is, the contributions made by photons scattered into the line of sight by the aerosol. The smaller radiances for the distant target at high reflectances are due to the aerosol scattering photons away from the line of sight once they have been reflected from the target. These contributions and depletions can be thought of as occurring because

objects tend toward the equilibrium radiance as the objects are moved farther from the observer.

TABLE 10

Target radiance as a function of reflectivity using 800 photons/line of sight.

	TARGET REFLECTIVITY		
Target	0.15	0.45	0.75
Aerosol			
Far	0.1079	0.1750	0.2477
Near	0.07091	0.1738	0.2848
Difference	0.03699	0.00120	(0.03710)
Rayleigh			
Far	0.1095	0.2070	0.3091
Near	0.07605	0.1903	0.3135
Difference	0.03345	0.1670	(0.00440)

Some idea of the value of the equilibrium radiance can be gleaned from table 10. For the aerosol case, there is little difference in target radiances for the near and far target when the target reflectance is 0.45. Therefore, the sky is neither depleting nor contributing to the target radiance. The target radiance value where this occurs is very close to the equilibrium radiance of the scene. On the other hand, the target reflectance for the Rayleigh case where there is little change between the far and near targets occurs at 0.75. Therefore, we would expect the Rayleigh equilibrium radiance to be larger than the aerosol equilibrium radiance for the sun in a theory left configuration.

In order to specifically compute the equilibrium radiance, all targets were removed from the canyon depiction and the observer's line of sight was varied through ten degrees of azimuth from minus five degrees to plus five degrees at zero degrees elevation. Using the mean radiance values from table 1, figure 11 shows the fairly noisy aerosol equilibrium radiances for the morning case. Because we would expect the equilibrium radiance to vary smoothly in a featureless vista as an observer scanned from left to right, a simple averaging scheme consisting of a three point arithmetic average about the radiance value being considered was performed to smooth the computed mean radiances. The resulting points, shown in the same figure, are fit very closely by the aerosol's phase function. Anticipating future needs, 0.3705 and 0.4390 are taken to be representative equilibrium radiance values for left and right of zero degree azimuth viewing. Both average values approximate computed radiances to within ten percent.

An interesting phenomenon emerges when only first order scatters are plotted from run number one of table 1 (see figure 12). The points are found to vary according to the aerosol's phase function as they should. Thus, the noise from the multiple scatters appears to be coming from higher order scatter events. For first order scatters, unless the observer is looking directly at the sun, any photons reaching his eyes must first undergo one scatter by the aerosol. Therefore the aerosol is behaving like a source and we are essentially observing the aerosol's phase function. When we include higher order scatters, the aerosol can behave either as a source, deflecting photons into the line of sight again, or as a sink, deflecting photons away from the line of sight. Therefore, along one line of sight, higher order scatters may act to

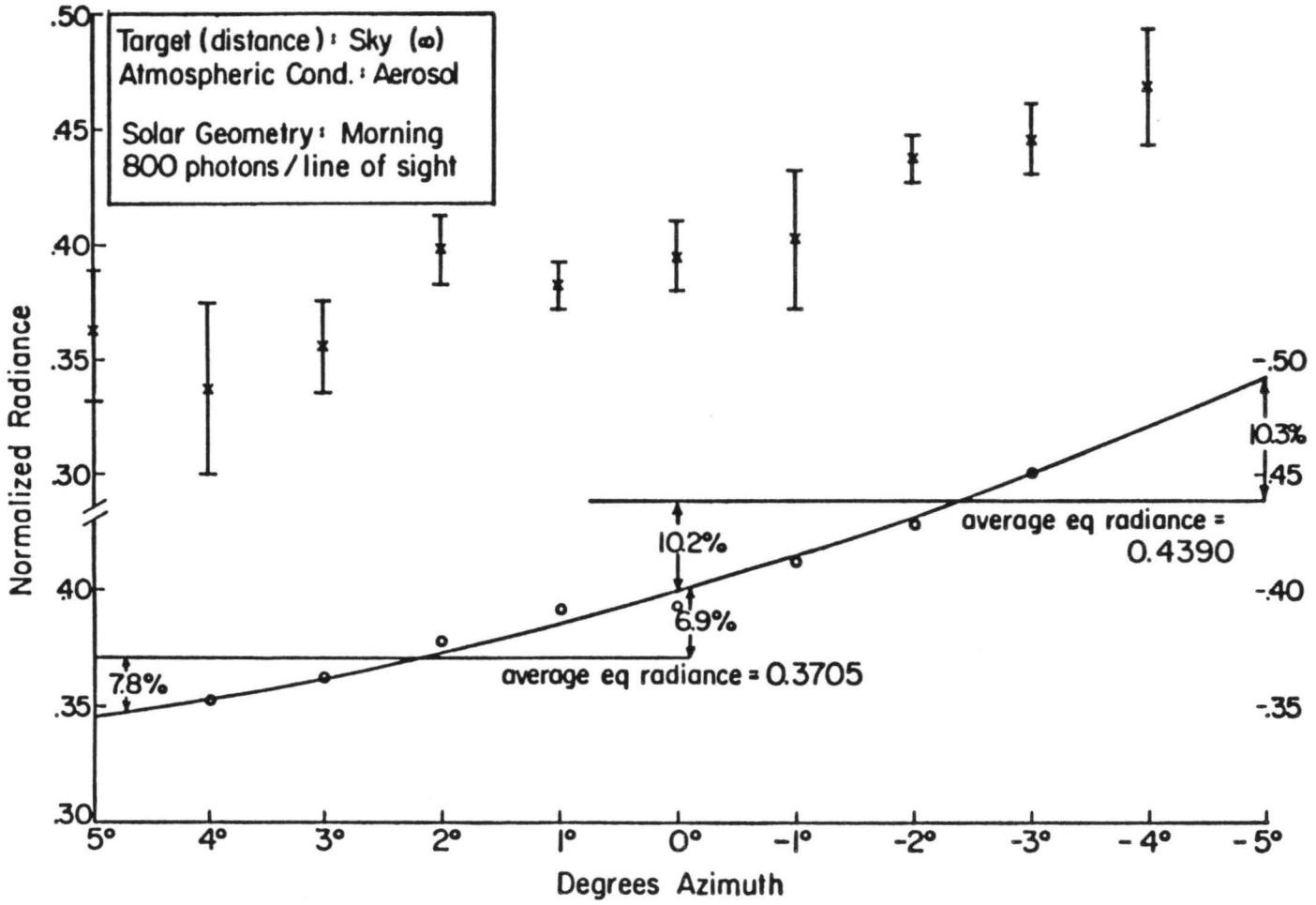

Figure 11. Aerosol morning equilibrium radiances plotted as a function of observer azimuth angle. X's represent unsmoothed radiance values from table 1 and °'s represent smoothed radiance values from table 1.

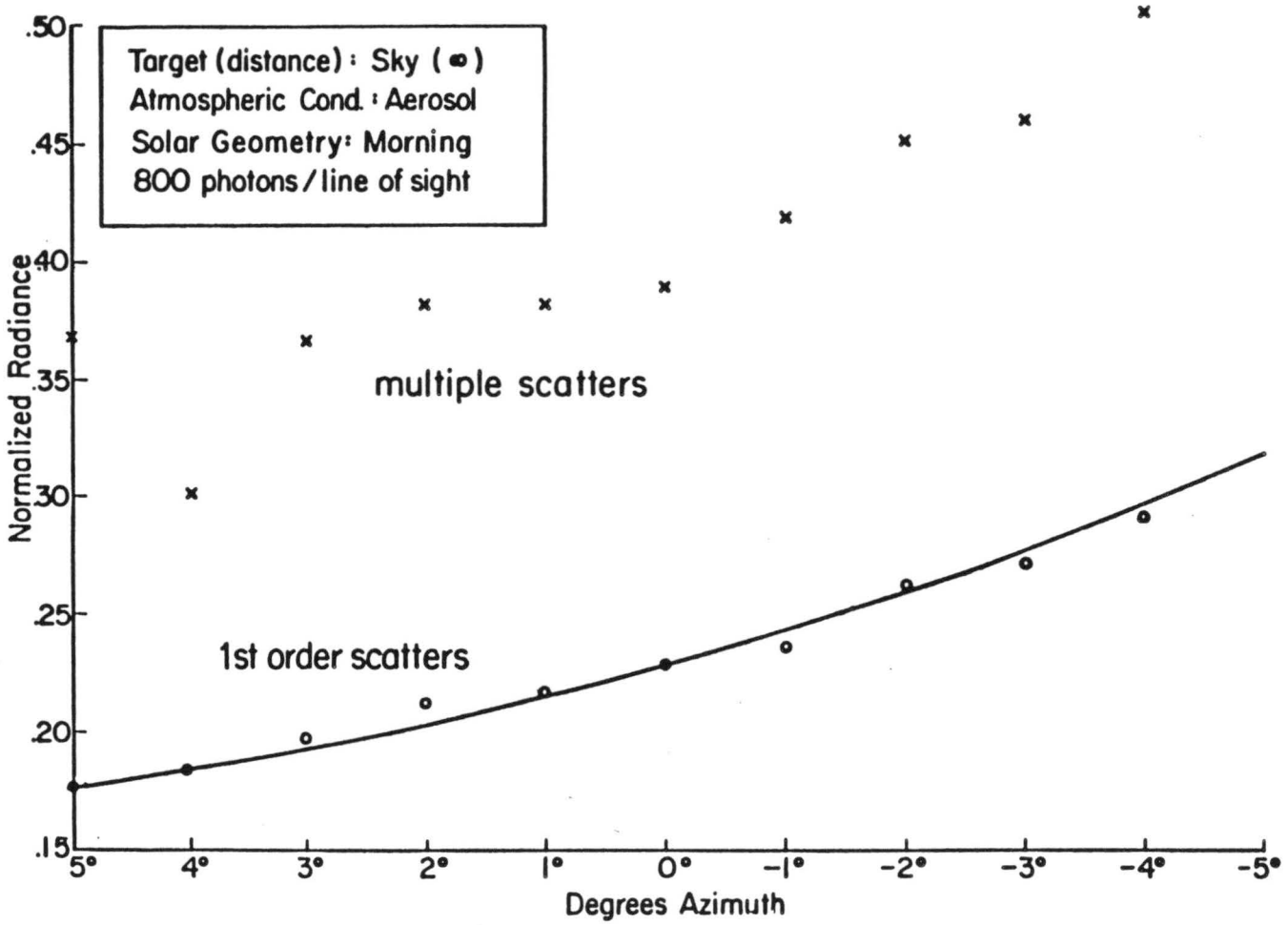

Figure 12. Aerosol morning equilibrium radiances from run one of table 1 plotted as a function of observer azimuth angle for a multiple order scatter model and a single order scatter model.

enhance the radiation reaching the observer while along an adjacent line of sight, higher order scatters may act to diminish it, thus leading to fairly noisy results. It is also important to note that to accurately simulate Grand Canyon radiance values, a first order scatter model would not be sufficient since there are significant contributions of higher order scatter events to the radiance values.

Although the radiance values derived from a first order scatter model are too low, the apparent spectral contrast values are within ten percent of the apparent spectral contrast values derived from the multiple scatter model as shown in table 11. However, the first order scatter model underestimates the illuminated target's apparent spectral contrast while it overestimates the shadowed target's apparent spectral contrast. Therefore, the contiguous spectral contrasts derived from the first order scatter model have a larger error. The reason for this can be seen by rewriting the equation which relates C_c to C_r using absolute values since in the context of this study, C_r is always negative:

$$C_c = |C_r(\text{dark})| - |C_r(\text{light})| \; / \; [1 - |C_r(\text{dark})|].$$

Because the dark target contrasts are overestimated and the light target contrasts are underestimated, the numerator in this expression will be significantly larger for a first order scatter model than for a multiple order scatter model while the denominator will be only slightly larger for a first order scatter model. The end result will be to produce larger errors in the contiguous spectral contrasts derived from a first order scatter model.

TABLE 11

Comparison of contrasts derived from a first order scatter model and a multiple order scatter model

target	first order	multiple order	% diff
apparent spectral contrast			
morning I	-0.563	-0.547	2.9
morning B	-0.941	-0.928	1.4
theory left I(ill)	-0.380	-0.421	-9.7
theory left I(shad)	-0.626	-0.585	7.0
theory right B(ill)	-0.678	-0.703	-3.6
theory right B(shad)	-0.947	-0.888	6.6
contiguous spectral contrast			
theory left I	0.396	0.283	39.9
theory right B	0.836	0.622	34.4

The underestimate of the apparent spectral contrast for illuminated targets and the overestimate for shadowed targets can be explained by considering the concept of equilibrium radiance. In a multiple order scatter model, the atmosphere scatters a net number of photons away from the line of sight of the observer for inherent target radiances which are less than the equilibrium radiance, and scatters a net number of photons into the line of sight for inherent target radiances which are

greater than the equilibrium radiance. A first order scatter model will then overestimate the illuminated target's radiance because it does not allow the atmosphere to deplete the inherent target radiance. Therefore, the apparent spectral contrast of the illuminated target will be underestimated. Conversely, a first order scatter model will overestimate the apparent spectral contrast for the shadowed target since it does not allow the atmosphere to enhance the inherent target radiance.

Figure 13 shows the morning Rayleigh equilibrium radiances. The results for each line of sight are consistent with each other and an average value of 0.2669 can be taken as a representative equilibrium radiance. Similarly, in the afternoon, the aerosol equilibrium radiance computations are well behaved in the domain as shown in figure 14 and we are therefore justified in taking an average value of 0.1418. The average equilibrium radiance for a Rayleigh atmosphere in the afternoon was computed to be 0.2250 as in figure 14.

Equlilibrium radiances were also calculated for an aerosol and Rayleigh atmosphere for the sun in a theory left configuration. The results, shown in figure 15 indicate a mean aerosol equilibrium radiance of 0.1939 and a mean Rayleigh equilibrium radiance of 0.3141. These results are consistant with the values expected to be found when looking at table 10. Targets with radiances larger than this value, then, will grow darker as they are moved away and targets with radiances smaller than this value will grow lighter as they are moved away. Figure 16 shows the results for aerosol and Rayleigh atmosheres with the sun in a theory right geometry. Mean equilibrium radiances are 0.1881 and 0.3159 for the aerosol and Rayleigh cases, respectively.

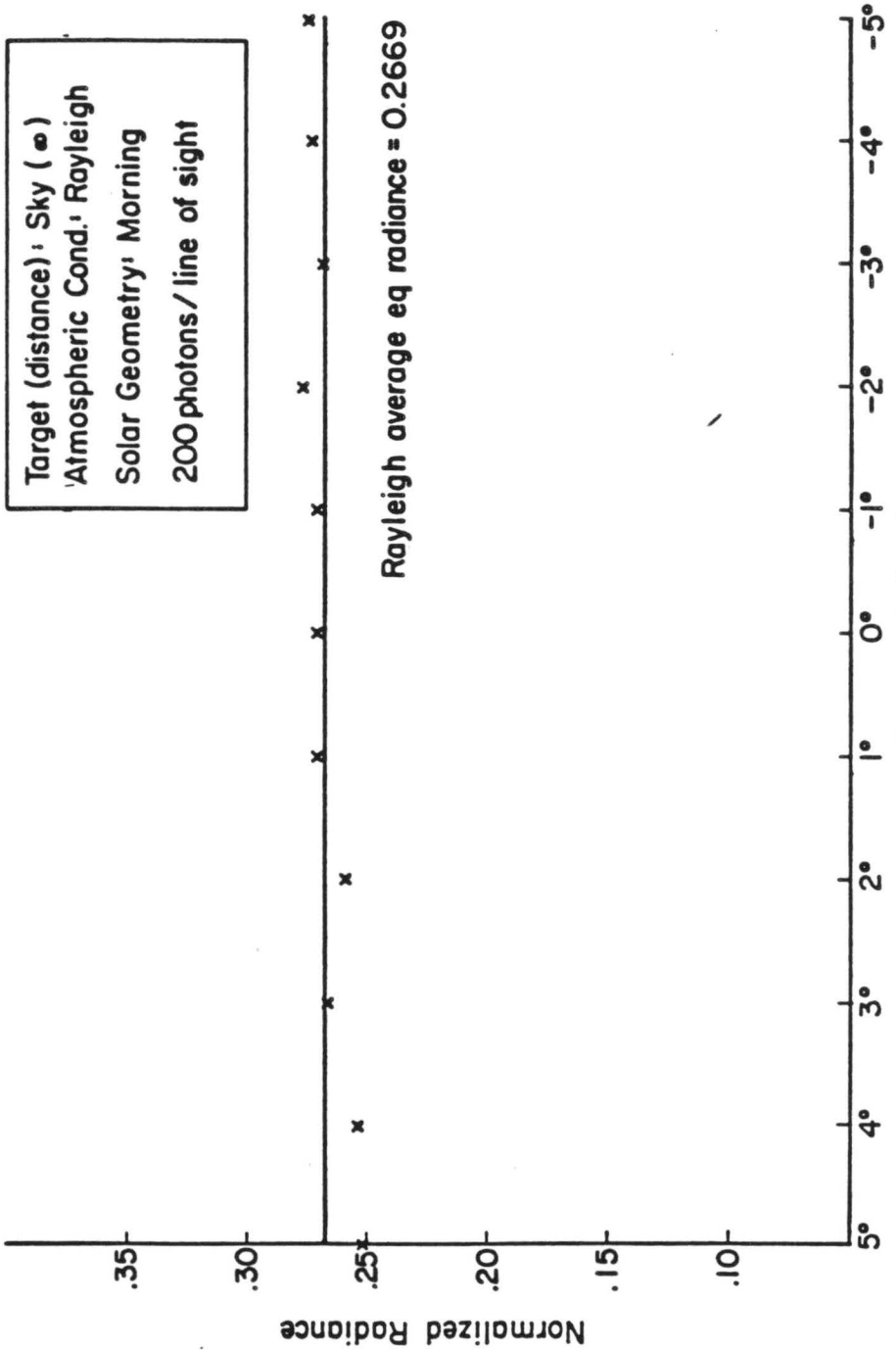

Figure 13. Rayleigh morning equilibrium radiances plotted as a function of observer azimuth angle.

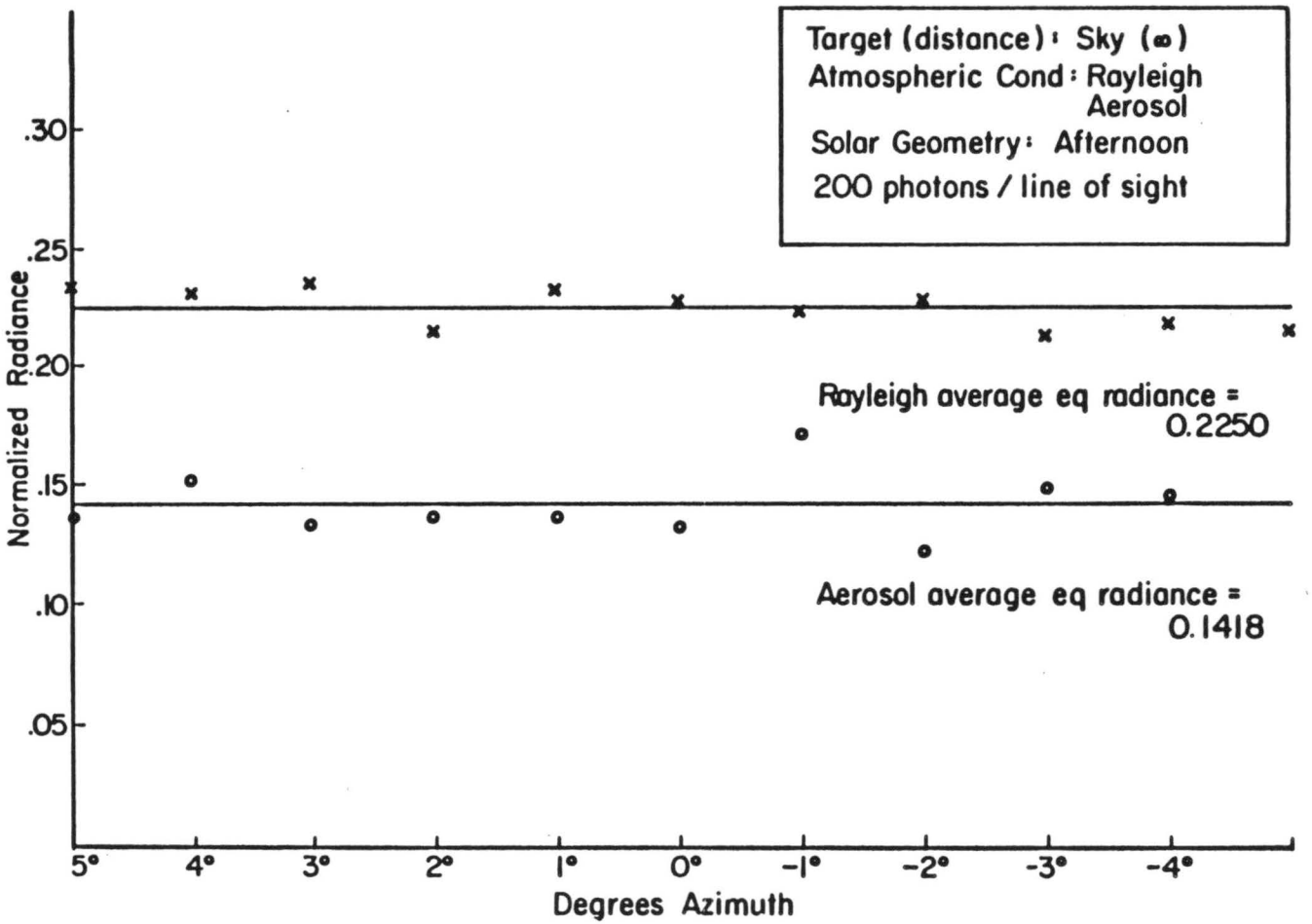

Figure 14. Rayleigh and aerosol afternoon equilibrium radiances plotted as a function of observer azimuth angle.

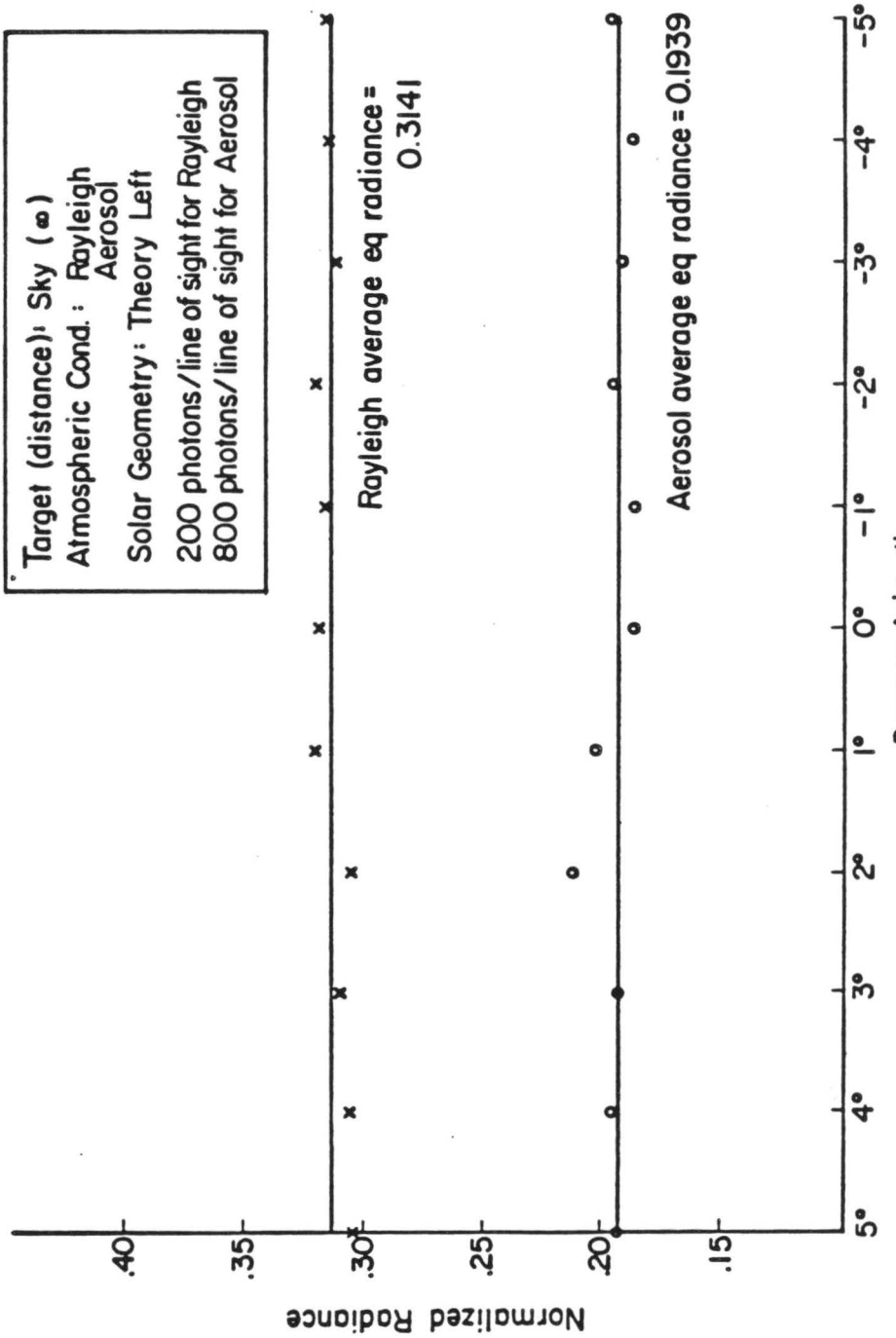

Figure 15. Rayleigh and aerosol theory left equilibrium radiances plotted as a function of observer azimuth angle.

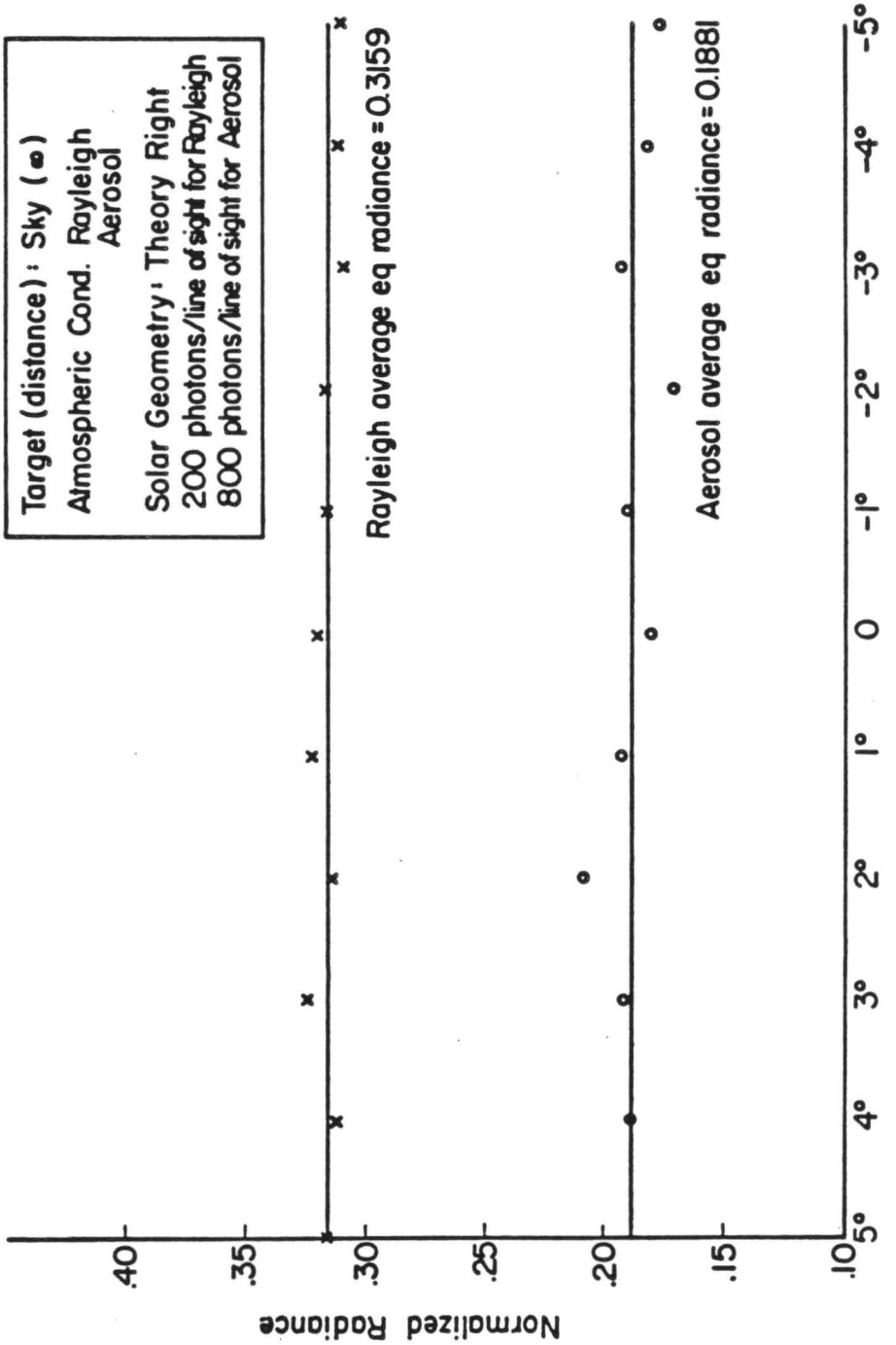

Figure 16. Rayleigh and aerosol theory right equilibrium radiances plotted as a function of observer azimuth angle

The equilibrium radiance for an aerosol atmosphere is 0.1418 for the afternoon case which is considerably smaller than the 0.2550 value for a Rayleigh atmosphere. The equilibrium radiance for an aerosol atmosphere is lower than that for a Rayleigh atmosphere because in the afternoon, the sun is positioned behind the observer. Since the aerosol is strongly forward scattering, relatively little light would be back scattered to the observer and the equilibrium radiance would be correspondingly smaller. In the morning, though, when the observer is looking toward the sun, the equilibrium radiance for the aerosol is considerably larger than the 0.2503 for a Rayleigh atmosphere. This is to be expected from an aerosol with strong forward scattering characteristics. The parameterized equilibrium radiances are summarized in table 11 for all the sun geometries examined for use in the following section.

TABLE 12

Summary of the parameterized equilibrium radiances

sun geometry	eq. radiance
aerosol morning	0.3705 / 0.4390
Rayleigh morning	0.1418
aerosol theory left	0.1939
Rayleigh theory left	0.3141
aerosol theory right	0.1881
Rayleigh theory right	0.3159
aerosol afternoon	0.1418
Rayleigh afternoon	0.2550

3.4.0 The Koschmieder Estimate

The Koschmieder equation is strictly valid only under the three restrictions mentioned in section 2.3. In order to determine the sensitivity of the Koschmieder equation to these assumptions, each assumption was investigated under both aerosol and Rayleigh atmospheric conditions using morning and afternoon solar geometries. The equilibrium radiances used for the Koschmieder estimate are those parameterized in section 3.3 and summarized in table 12.

3.4.1 Horizontal Path

Because the extinction coefficients are layered with height in this model, an observer's line of sight will not, in general, pass through an atmospheric layer consisting of a constant extinction coefficient.

Therefore, the line of sight must be horizontal in order that the extinction coefficient not vary. To investigate the importance of a constant extinction coefficient as it relates to the Koschmieder estimate, relative differences between Koschmieder and model generated radiances were compared for horizontal and oblique lines of sight.

In order to employ the Koschmieder equation for an oblique line of sight, the optical depths should be layer weighted so that the observer was effectively looking horizontally through a layer of constant optical depth. These layer weighted optical depths are given in table 13, where Z1 and Z2 represent the bottom and top of the atmospheric layer being considered, Z1 - Z2 represent the layer's thickness, and beta represents the extinction characteristics of that layer. To obtain N(0), the observer was placed ten meters from the target and the radiance was computed. The results of the computer runs, as well as comparisons with model generated radiances, are shown in table 14.

TABLE 13

Layer Weighted Optical Depths

Z1(km)	Z2(km)	Z2 - Z1(km)	beta(Ray) (1/km)	beta(Aer) (1/km)
1.30	1.43	0.13	0.01194	0.04731
1.43	1.58	0.15	0.01052	0.03455
1.58	1.70	0.12	0.01033	0.03278
1.70	1.83	0.13	0.01019	0.03149
1.83	2.11	0.28	0.00995	0.0301
2.11	2.269	0.159	0.00971	0.02755

tau(I,Ray)	0.219
tau(I,Aer)	0.702
tau(B,Ray)	0.059
tau(B,Aer)	0.175

TABLE 14

Oblique lines of sight using 800 photons/line of sight for the afternoon and 3200 photons/line of sight for the morning.

target	time	tau	N(q)	N(O)	N(kosch)	N(model)	% diff
B(Ray)	afternoon	0.059	0.2250	0.002676	0.0154	0.00962	60
B(Aer)	afternoon	0.175	0.1418	0.002704	0.0250	0.01215	106
B(Ray)	morning	0.059	0.2669	0.003560	0.0186	0.01011	84
B(Aer)	morning	0.175	0.3705	0.003074	0.0621	0.02268	174
I(Ray)	afternoon	0.219	0.2250	0.06724	0.0983	0.07667	28
I(Aer)	afternoon	0.702	0.1418	0.06292	0.1027	0.08883	16
I(Ray)	morning	0.219	0.2669	0.003631	0.0554	0.04886	13
I(Aer)	morning	0.702	0.3705	0.007817	0.1908	0.1442	32

To obtain a literally horizontal line of sight, the simulated observer position was lowered when looking at target 'B' and raised when looking at target 'I' so that the lines of sight became horizontal. The optical depths used in the Koschmieder estimate are shown in table 15 and the resulting recalculations are shown in table 16. The horizontal optical depths are larger for target 'B' because the lowered observer is looking through an optically thicker layer of exponentially scaled aerosol and smaller for target 'I' because the raised observer is looking through an optically thinner layer of aerosol.

TABLE 15

Horizontal Optical Depths

Atmosphere type	beta	path length	tau
I(Ray)	0.00995	22 km	0.219
I(Aer)	0.03031	22 km	0.662
B(Ray)	0.0102	6 km	0.061
B(Aer)	0.0315	6 km	0.189

TABLE 16

Horizontal lines of sight using 800 photons/line of sight for the afternoon and 3200 photons/line of sight for the morning.

target	time	tau	N(q)	N(O)	N(kosh)	N(model)	% diff
B(Ray)	afternoon	0.061	0.2250	0.002676	0.0158	0.004816	228
B(Aer)	afternoon	0.189	0.1418	0.002704	0.0267	0.009011	196
B(Ray)	morning	0.061	0.2669	0.003560	0.0191	0.004487	-77
B(aer)	morning	0.189	0.3705	0.003074	0.0663	0.01034	542
I(Ray)	afternoon	0.219	0.2250	0.06724	0.0983	0.07505	31
I(Aer)	afternoon	0.662	0.1418	0.06292	0.1011	0.07294	39
I(Ray)	morning	0.219	0.2669	0.003631	0.0554	0.04945	12
I(Aer)	morning	0.662	0.3705	0.007817	0.1834	0.1343	37

If we compare the percent difference columns of tables 14 and 16, we find that for feature 'I', there is no significant improvement in the Koschmieder estimate when the line of sight becomes horizontal. In fact, the percent difference for the afternoon aerosol case is twice as large. Therefore, this particular assumption is not significantly violated in the Grand Canyon model because the lines of sight are only slightly depressed. Target 'B' will be discussed below.

3.4.2 Uniformly Lighted Region

The results for target 'B' in table 16 indicate a large error because the line of sight lies in the shade, excluding radiance contributions from most, if not all, higher order scatter events. Thus the Koschmieder equation overestimates the radiance contribution from path light and is unreliable when the line of sight lies in the shade. Therefore, the assumption that the path lie in a uniformly lighted region is critical for this particular geometry and probably most others.

3.4.3 Radiance Distribution with Height

In order to determine the sensitivity of the Koschmieder estimate to a vertically invarient radiance distribution along the path length, the Koschmieder estimate was tested with the sun in either a theory left or theory right configuration so that appropriate portions of targets 'B' and 'I' were shadowed. The results, shown in table 17, can be explained by referring to the Koschmieder equation in the simpler form:

$$N = N(0) * T + N(q) * S.$$

T is the transmission coefficient, representing the fraction of light transmitted along the line of sight through the medium, and S is the

scattering coefficient, representing the fraction of light scattered into the line of sight by the medium. When no absorption is present, as in this study, T + S = 1.0.

TABLE 17

Koschmeider estimates for contiguous spectral contrasts using 800 photons/line of sight.

target	tau	N(q)	N(O)	N(kosh)	N(model)	% diff
----I----						
shad aer	0.702	0.1939	0.01085	0.1032	0.07034	46.7
illum aer	0.702	0.1939	0.06259	0.1288	0.1079	19.4
shad Ray	0.219	0.3141	0.003858	0.06488	0.05640	15.0
illum Ray	0.219	0.3141	0.06798	0.1164	0.1095	6.3
----B----						
shad aer	0.175	0.1881	0.01371	0.0417	0.02681	55.5
illum aer	0.175	0.1881	0.06085	0.0813	0.07091	14.7
shad Ray	0.059	0.3159	0.001957	0.0199	0.01951	2.0
illum Ray	0.059	0.3159	0.06168	0.0762	0.07605	.2

From table 17, it is obvious that the Koschmieder estimate handles the Rayleigh cases better than the aerosol cases; likewise the illuminated target results are better than the shadowed target results. When the optical depths are large, as in the aerosol cases, the scattering term is large, thus heavily weighting the equilibrium radiances. This heavy weighting of the equilibrium radiance forces discrepancies between model generated radiances and Koschmieder

generated radiances. When the equilibrium radiance terms are weighted less heavily, as in the Rayleigh cases, the Koschmieder estimate is more accurate. Because the inherent target radiances for the shadowed areas are very low and are subject to larger coefficients of variation than the illuminated targets, the Koschmieder estimate appears to handle shadowed areas less accurately than illuminated areas.

The Koschmieder equation performs well when the equilibrium radiance value contributes relatively little to the apparent radiance of the target. This occurs when the scattering coefficient is small, thus we must conclude that the N(q)*S term does not treat the physics of the scattering process correctly. The fault is the violation of the assumption used to derive the Koschmieder equation that radiance values are independent of height. Because radiance values do vary with height, the equilibrium radiance term is not constant along the path length and the scattering term must be represented by an integral rather than the simple product N(q)*S.

3.4.4 Koschmieder Contrasts

Since the human eye is more sensitive to contrasts than to actual radiance values, contiguous target contrast using the Koschmieder estimate were compared to those generated from the model using data from table 17. The results, shown in table 18, indicate better agreement between model and Koschmieder contrasts than between model and Koschmieder radiances. In fact, all contiguous contrasts are accurate to the order of ten percent except when the illuminated portions of targets 'I' and 'B' are compared to the shadowed portions in an aerosol atmosphere, and when the shadowed portions of targets 'I' and 'B' are compared. In the aerosol case, there are large errors in the shadowed

portion of target 'I' and target 'B' so that contiguous contrasts incorporating these values are expected to be in error. However, these errors can cancel each other out in division as in the aerosol case comparing the shadowed areas of 'I' and 'B'. In the Rayleigh case, a thirteen percent overestimate occurs because of the relatively large error in estimating the radiance from the shadowed portion of target 'I'.

TABLE 18

Contiguous target contrasts.

target contrast	atmosphere type	Koschmieder	model	% diff
I(light)/I(dark)	Rayleigh	1.79	1.94	-7.7
	Aerosol	1.25	1.53	-18.3
B(light)/B(dark)	Rayleigh	3.83	3.90	-1.8
	Aerosol	1.95	2.64	-2
I(light)/B(light)	Rayleigh	1.53	1.44	6.2
	Aerosol	1.58	1.52	
I(dark)/B(dark)	Rayleigh	3.26	2.89	12.8
	Aerosol	2.47	2.62	-5.7

The Koschmieder estimate performed better when used with the contiguous contrasts because the ratio removed any bias in the estimate. In this particular case, a bias seemed to be present since the Koschmieder equation overestimated the radiances of all the targets in a similar way, as can be seen in table 17. However, as seen in some other sun geometries, the Koschmieder estimate does not consistently

overestimate radiances, thus decreasing the effectiveness of the contiguous spectral contrast in removing bias.

IV. CONCLUSION

Using a backward version of the Monte Carlo Radiative Transfer model, radiance values in the Grand Canyon were simulated to within the precision of ten percent. Target and sky radiance values were computed using solar geometries which placed the sun in front of and behind the observer. It was found that 3200 photons were needed for solar geometries with the sun in front of the observer and 800 photons were needed for solar geometries with the sun behind the observer to obtain standard deviations that were not more than ten percent of the mean calculated radiance values.

Target radiances were examined as a function of target reflectance to determine that the aerosol affects target radiance values in some cases by the addition of path light. In other cases, the aerosol depletes target radiances by scattering a net number of photons away from the line of sight of the observer. Target radiances were also examined as a function of foreground reflectance. Apparent target radiances increased as the foreground reflectance increased because the foreground was behaving as a source and illuminating the Grand Canyon scene from below. The apparent spectral contrast was found to increase with increasing foreground reflectance while the contiguous spectral contrast was found to decrease with increasing foreground reflectance. Because one would expect the target's features to become indistinct as the aerosol adds path light to the line of sight, the contiguous spectral contrast becomes a valuable tool in evaluating visibility.

Variations in the observer geometry were also investigated and in general, visibility was found to be better when viewed from the south rim of the canyon due to the nature of the aerosol phase function and the observer-sun geometry.

Equilibrium radiances were calculated for each of the sun geometries considered in the model. Average values of the equilibrium radiance were incorporated into the Koschmieder estimate to investigate the three assumptions used to derive Koschmieder's equation. The Koschmieder estimate was deemed to be of limited value since the path did need to be uniformly lighted and the radiance values did need to be independant of height. In addition, the contiguous target contrasts were deemed useful when used with the Koschmieder estimate because they tended to remove a bias which seemed to be present in the Koschmieder radiances.

Finally, it was shown that it is imperative that a multiple order scatter model be used when representing radiance values in the Grand Canyon. Although the apparent spectral contrasts derived from a single order scatter model were within ten percent of those values obtained from the multiple order scatter model, the contiguous spectral contrasts were in large error.

REFERENCES

Collins, D. G., W. G. Blattner, M. B. Wells, and H. G. Horak, 1972: Backward Monte Carlo Characteristics of the Radiation Emerging from Spherical-Shell Atmospheres. Appl. Optics., 11, 2684-2696.

Davis, J. M. and S. K. Cox, 1982: Reflected Solar Radiances from Regional Scale Scenes. J. Appl. Met., 21, 1698-1712.

Davis, J. M., T. B. McKee, and S. K. Cox, 1985: An Investigation of the Application of the Monte Carlo Method to Problems in Visibility Using a Local Estimate. Appl. Optics, accepted for publication.

Deirmendjian, D., 1969: Electromagnetic Scattering on Spherical Poly-dispersions. Elsevier, 290 pp.

Duntley, S. Q., A. R. Boileau, and R. W. Preisendorfer, 1957: Image Transmission by the Troposphere I. J. Opt. Soc. Am., 47, 499-506.

Elterman, L., 1970: Vertical attenuation model with Eight Surface Meteorlogical Ranges 2 to 13 Kilometers. AFCRL-70-0200.

Malm, W. C., 1979: Considerations in the Measurement of Visibility. APCA J., 29, 1042-1052.

McClatchey, R. A., R. W. Fenn, J. E. Selby, F. E. Voltz, and J. S. Garing, 1971: Optical Properties of the Atmosphere (Revised). AFCRL-71-0279.

Preisendorfer, R. W., 1976: Hydrologic Optics. Vol. III. NOAA, Joint Tsunami Research Effort, Honolulu, Hawaii, 246 pp.